AVIATION RESEARCH LABORATORY

INSTITUTE OF AVIATION

UNIVERSITY OF ILLINOIS AT URBANA-CHAMPAIGN

FINAL REPORT

THE DEVELOPMENT OF METHODS FOR PREDICTING AND MEASURING DISTRIBUTION PATTERNS OF AERIAL SPRAYS*

ALLEN I. ORMSBEE
MICHAEL B. BRAGG
MARK D. MAUGHMER

REPORT ARL 79-1

JUNE 1979

*Sponsored in part by NASA Langely Research Center under grant NSG 1434

Aviation Research Laboratory
Institute of Aviation
University of Illinois at Urbana-Champaign

Report ARL 79-1

Final Report

THE DEVELOPMENT OF METHODS FOR PREDICTING AND MEASURING DISTRIBUTION PATTERNS OF AERIAL SPRAYS*

Allen I. Ormsbee
Michael B. Bragg
Mark D. Maughmer

June 1979

*Sponsored in part by NASA Langley Research Center under grant NSG 1434

The Development of Methods for Predicting and Measuring Distribution Patterns of Aerial Sprays

Allen I. Ormsbee
Michael B. Bragg
Mark D. Maughmer

ABSTRACT

The research effort reported on in this paper is directed toward establishing techniques of small-scale model testing for the purpose of developing aerial application systems. In particular, the capability of conducting scale model experiments which involve the ejection of small particles into the wake of an aircraft close to the ground is developed.

A set of relationships used to scale small-sized dispersion studies to full-size results are experimentally verified and, with some qualifications, basic deposition patterns are presented. In the process of validating these scaling laws, the basic experimental techniques used in conducting such studies, both with and without an operational propeller, were developed. The procedures that evolved are outlined in some detail. Lastly, the envelope of test conditions that can be accommodated in the Langley Vortex Research Facility, which were developed theoretically, are verified using a series of vortex trajectory experiments that help to define the limitations due to wall interference effects for models of different sizes.

TABLE OF CONTENTS

NOMENCLATURE

AR	Wing aspect ratio, b^2/S
C_D	Drag coefficient, D/qS
C_L	Lift coefficient, L/qS
C_T	Thrust coefficient, $T/\rho n^2 d^4$
D	Drag force
H	Model height (wing tip), semispans
J	Advance ratio, U_∞/nd
L	Lift force
S	Wing area
T	Propeller thrust
U_∞	Free stream velocity (model speed)
b	Wing span
d	Propeller diameter
g	Gravitational vector
h	Model height (wing tip), semispans
n	Propeller angular velocity, rpm
q	Dynamic pressure, $\frac{1}{2}\rho U_\infty^2$
t	Time
z_o	Initial particle position (ejector height), semispans
Γ	Characteristic circulation for the wing
Γ_p	Characteristic circulation for the propeller
Θ_p	Instantaneous angular position of the propeller
α	Aircraft angle of attack

δ	Particle diameter
μ	Absolute air viscosity
ρ	Air density

INTRODUCTION

Currently, the National Aeronautics and Space Administration is engaged in research directed at advancing aerial applications technology. One aspect of this program, as reported in reference 1, is aimed at increasing the understanding of the interaction of a dispersed spray with the aircraft wake. The ultimate objective of this research is to develop the capability of modifying the aircraft wake characteristics and the dispersal system in such a manner as to produce a wide, uniform deposition pattern, and, if possible, minimize the drift problem as well. Although some full-scale agricultural aircraft deposition data has been obtained, the large number of variables which are difficult to control in such experiments cause these data to be of limited value. Thus, it is felt that strictly controlled scale model tests could be most useful in a systematic investigation of the wake-dispersal interaction. The development of the capability to simulate full-scale models should provide a highly efficient research tool to generate baseline data, which is not currently available, as well as to provide a means by which future advanced aircraft configurations and dispersal concepts may be evaluated.

In order to permit the results of scale model tests to be extrapolated to full-scale conditions, scaling laws have been derived (references 2 and 3) which apply to the trajectory of a particle ejected into the wake of an aircraft. The analysis utilized in those studies is concerned with nearly spherical droplets in the 100 to 500 micron diameter size range and concludes that to insure the same non-dimensional particle trajectory in the wake of a geometrically scaled aircraft, the following parameters must be held constant between full-scale and the model:

$$\frac{U_\infty^2}{bg}, \frac{\Gamma}{U_\infty b}, \frac{U_\infty t}{b}, \frac{h}{b}, \frac{\Gamma}{\Gamma_p}, \frac{U_\infty}{nd}, \frac{d}{b}, \Theta_p, \frac{\rho^{1+\gamma}\,\delta^{\gamma-1}\,U_\infty^{2+\gamma}}{\sigma g \mu^\gamma}$$

The first quantity indicated above is the square of the Froude number and determines the model test velocity. The second parameter is the non-dimensional vortex strength for which constancy is ensured if C_L/AR is held constant. For a geometrically scaled model and assuming Reynolds and Mach number independence, this constraint reduces to operation at constant aircraft angle of attack. Non-dimensional time is represented by the third term, while the fourth represents the non-dimensional height of the aircraft above the ground plane. The next four parameters concern the proper scaling of the propeller slipstream and are, respectively, the ratio of the wing to propeller vortex strengths, the advance ratio, the geometric scale of the propeller diameter, and the angular orientation of the propeller when the particle is introduced into the flow. The last term shown fixes the relationship between the size and density of the scaled particles and results from the introduction of the particle drag curve as approximated by $C_D = BR^\gamma$, where B and γ are constants that are determined for the range of particle Reynolds numbers of interest.

The primary goal of the research effort herein reported was to validate the particle trajectory scaling laws. In addition, the program was concerned with developing experimental techniques for the testing of scale model agricultural aircraft systems in the NASA/Langley Vortex Research Facility. Thus, the envelope of possible test conditions was examined and the limitations of the facility, including those due to Reynolds number and wall effects, were considered.

It should be emphasized that the test simulitude as developed is only concerned with scaling the trajectory of a single particle, and hence, interference between particles is ignored. Further, no attempt was made to

scale nozzle operation and the purpose of the model ejectors in these experiments was merely to place a particle at a given initial point in the wake of the aircraft. Thus, the data obtained strictly applies only to the validation of the scaling laws and should not be construed as an indication of baseline deposition information. The fact that the broad single-ejector deposition patterns occur at all in these tests only reflects experimental errors associated with the exact sizing of the particles, the mutual interference between particles deposited in the wake, and the inability to impart to the particles precisely the same initial conditions.

FACILITY DESCRIPTION

Unlike conventional wind tunnels in which the model is held fixed in a stream of forced air, the Langley Vortex Research Facility, shown in figure 1, is unique in that data is obtained by moving the test model through stationary air; a feature essential in the study of ground deposition patterns behind an agricultural aircraft. By injecting smoke into the test section of the facility, observation of the vortex wake of a passing model aircraft is also possible.

The facility consists of an enclosed overhead track 550 m long. The model is mounted on a strut below a streamlined power carriage which travels along the track at test velocities of up to 30 m/sec. The strut itself allows the model to be adjusted in height above the ground plane, as well as in pitch attitude, and incorporates a six-component strain gage balance for force data. The test section, in which measurements and smoke studies are made, has been constructed to isolate the wake of the model from the carriage. The test section is 91 m long, 5.5 m wide, and 5.2 m high with a 5 cm wide opening in the ceiling to allow the supporting strut to pass. Before the entrance to the test section, the carriage has 305 m to accelerate to a prescribed speed which is then maintained at a constant value through the test section. Upon leaving the test section, caliper brakes are applied to provide a 1 g deceleration over the last 76 m of the track. Additional details concerning the characteristics of this facility are presented in reference 1.

MODEL DESCRIPTION

Because meaningful full-scale data was unavailable, the experimental program to validate the scaling laws had to be self-contained. Thus, it was decided to examine the single-ejector ground depositions between geometrically scaled models with appropriate test conditions and particle characteristics dictated by the scaling laws. Essentially, only two different sized models were required for confirmation of the scaling laws; however, as a further objective of the experiments was to determine the maximum model span for which the adverse effects of the test section walls are held within acceptable bounds, an additional relatively large model was included for which it was felt that wall effects would undoubtedly be observed. Therefore, the three wing-fuselage models shown in figure 2 were constructed with spans of 1.22 m (4 ft), 1.83 m (6 ft), and 2.44 m (8 ft). The models employ a rectangular wing platform with an aspect ratio of 6. The airfoil section in an NACA 4412 which, being flat-bottomed, facilitates the installation of the dispersal system. The design and test conditions for each model were determined by scaling them to a full-scale aircraft having a span of 12.2 m (40 ft) and a flight speed of 53.3 m/sec (119 mph). Thus, the three models represent scaling ratios of 0.10, 0.15, and 0.20 relative to the full-scale aircraft. The 0.10 scale model is shown, mounted on the adjustable strut above the test-section floor, in figure 3. As the wing-wake and the wing-fuselage intersection are the dominating features of an aircraft in determining particle trajectories, the scaling law validation models consist of only a wing and fuselage configuration without empennage components. The streamlined fuselage shell, of fineness ratio approximately

6.2, utilizes a circular cross-section throughout and has a maximum diameter of 0.208 semispans.

The dispersal system developed for the scaling law validation models consists of an inverted-cone shaped hopper which holds the particles that are then gravity-fed into a length of brass tubing which acts as the ejector. As the ejectors were not intended to simulate full-scale nozzles, the shape, operation, and flow field around the tubing were not scaled. The purpose of the ejectors is merely to deposit the particles in the aircraft wake at a point which is out of the wing boundary-layer introducing as little interference as possible. The ejector tubes are swept back at a forty-five degree angle from the mid-chord point such that the initial particle deposition point is 0.60 chord-lengths from the leading edge and 0.16 chord-lengths below the chordline. As shown in figure 4, the individual ejectors can be placed at different span-wise locations, including the model centerline. Operation of these ejectors is initiated by a simple but effective method that employs hook-equipped stoppers which are pulled from the ejectors by a trip-wire as the model enters the facility test section.

In addition to the configuration shown in figures 2, 3, and 4, all of the models are also capable of operating in a powered mode which includes a propeller to scale slipstream effects. The 0.10 and 0.15 scale versions of this mode are shown in figure 5. The carved wooden propellers were designed using the computer code developed at the University of Illinois and reported in reference 4. Operating parameters of the powered test models were based on a full-scale aircraft powerplant of 300 kw (401 hp), operating a 2.49 m (8.2 ft) diameter propeller at 2308 rpm with an 85% propeller efficiency. As required by the scaling laws, the thrust coefficient, C_T, of 0.068, and the advance ratio, J, of 0.56, were held constant between the models to

assure test similitude. The model propellers are driven by a pneumatic motor which is supplied with compressed air stored in the power carriage of the facility.

The purpose of the unpowered models in these experiments was to simplify the validation of the basic scaling laws without the added complications involved with data acquisition and reduction when an operational propeller is employed. After the particle dynamics and wake simulation were found to be properly scaled, the slipstream effects could then be incorporated to ascertain whether or not the desired non-dimensional behavior remains as required for the facility to be useful in future agricultural aircraft development.

PARTICLE SELECTION

The selection of the properly scaled particles to be used for each model in the scaling law validation experiments was based on an extensive search of commercially available candidates to determine which would most suitably scale to a common full-scale water droplet. Using a computer program to facilitate the iterative procedure required in calculating the scaling law parameters that fixes the relationship between the size and density of the particles, glass sphere microbeads were determined to most ideally fit the constraints of the experimental program. The characteristics of the glass spheres chosen for the initial scaling law validation, which correspond to a full-scale water droplet having a diameter of approximately 490 microns, are listed for each model in the following table:

SCALED GLASS BEAD PARTICLES

Model Scale	Particle Diameter (microns)	Particle Density (g/cm^3)	Full-Scale Water Droplet Diameter (microns)
0.10	105	2.42	477
0.15	125	2.42	496
0.20	105	3.99	502

The microbead particles that were utilized are 90% true spheres with only 2% irregularly shaped. For 98% of the particles, the diameters are within $\pm$ 10% of the values listed, while the densities are within $\pm$ 5%.

In order to obtain some understanding of the sensitivity of the particle trajectories to deviations from the proper scaling, ground deposition data was also obtained using glass bead particles which correspond to unsimilarly scaled full-size water droplets as indicated below:

UNSCALED GLASS BEAD PARTICLES

Model Scale	Particle Diameter (microns)	Particle Density (g/cm^3)	Full-Scale Water Droplet Diameter (microns)
0.15	105	2.42	390
0.15	125	2.42	490
0.15	105	3.99	580

Validation of the scaling laws throughout the full-scale droplet size range was examined by generating additional data for the 0.10 and 0.15 scale models using Fillite beads that scaled to full-size water droplets of a 200-micron diameter. The characteristics of these particles are:

SCALED FILLITE BEAD PARTICLES

Model Scale	Particle Diameter (microns)	Particle Density (g/cm^3)	Full-Scale Water Droplet Diameter (microns)
0.10	125	0.58	200
0.15	140	0.58	200

The diameters and densities of the Fillite particles are both within $\pm$ 5% of the given values.

The sensitivity of the ground deposition point of a particle to the variations in size and density of the beads used in the experiments was examined numerically using the trajectory computer codes of reference 2. The results indicate that a $\pm$ 10% variation in the diameter of a particle released at a spanwise location of 0.5 semispans results in a deposition width of $\pm$ 10% about the mean. For particles released at spanwise locations farther outboard, the deposition scatter becomes larger. The depositions spread similarly as a result of variations in particle density, although quantitatively, the sensitivity is about half of that caused by diameter variations. It was also concluded during these studies that,

rather than the spanwise mean value of an experimental deposition, the spanwise median of the pattern is more indicative of the proper ground deposition point of the scaled particle. This is because for the test particles used, only the average particle diameter and an estimate of the particle size range is known. Since no details of the particle size distribution are known, the best comparison with theory is to use the median deposition point that corresponds to the given average particle size. Furthermore, the spanwise median presents the best comparison between the three models as it is possible that the particles used in each of the three models have different size distribution patterns that would generate correspondingly different spanwise means, although the spanwise medians of the depositions in this case would still be identical. An additional justification for using the median of the distribution, rather than the mean, as the deposition point of a single particle is connected with the manner in which the experimental data were evaluated. Part of the data acquisition system utilized consists of a magnifying television camera that projects small portions of a single deposition pattern on a television screen, and the number of particles per unit of spanwise deposition length are manually counted by the experimenter. This procedure relies on the ability of the experimenter to distinguish visually between the uniform size and shape of the test particles and those of random noise inputs, such as dust. While this is not difficult near the center of the deposition, where many test particles for comparison are located, it becomes less reliable near the outer fringes of the deposition where only one or two particles are present. In the calculation of a mean spanwise location for the deposition, these values near the edges are weighted much more heavily than the more accurate data near the center and any error is consequently amplified. As the median value is defined as the spanwise location where half the particles in the deposition lie to the right and half to the left, it is only very

slightly affected by errors at the fringes. Thus, although the mean values of the depositions were calculated and found to not vary significantly from those of the median, the value of the spanwise median will be considered as the most reliable in comparing the results obtained in this research.

EXPERIMENTAL TECHNIQUE AND DATA REDUCTION

Particle Deposition Experiments

The primary experimental support for the validation of the particle trajectory scaling laws was obtained from a series of tests in which ground deposition patterns were compared between the three properly scaled particle sizes and models. To examine the influence of the vortex wake system behind the wing on the trajectory of a particle, deposition data were obtained for particles ejected at spanwise locations which include the model centerline, and from 0.2 to 0.7 semispans in one-tenth semispans increments. The baseline configuration for these experiments employs a model height of 0.51 semispans above the ground plane and a geometric angle of attack of nominally two degrees, such as to produce a lift coefficient of 0.61 which was maintained throughout the tests to within five percent.

The procedure utilized in collecting ejected particles for the scaling law investigation involved the placement of a narrow adhesive surfaced strip spanwise across the test section ground plane in such a manner that, as the model passed through the test section, the deposition from a single ejector would be fixed to the strip. To increase the reliability of the median values calculated from the depositions obtained for the unpowered model configurations, collector strips were employed for both right and left spanwise ejector locations on the model and the two results averaged. Furthermore, a low-frequency, lateral oscillation of the model-strut combination occurred as the carriage moved down the track. The period of the oscillation was determined for each model, and its influence nullified by locating two pairs of right and left ejector strips on the test section floor separated by a distance of one-half period.

For most of the baseline scaling law validation, the sampling size was increased by making a minimum of three runs for each ejector location on each model. These results were then combined to obtain a single average ejector deposition pattern and median value. The actual analysis of the particle deposition strips was facilitated by the previously described video-magnifying system and was used to determine the actual particle concentrations, in terms of percent of total particles deposited, as a function of the lateral location, in terms of semispans, at which they landed on the ground plane.

Vortex Trajectory Experiments

The purpose of the vortex trajectory experiments in this research was to aid in developing the boundaries of the facility test envelope. When an aircraft is in close ground proximity, the most significant influence of the ground on the wake system is to restrict its normal vertical descent and induce a rapid lateral outward movement of the system over the ground. The speed with which the lateral transport occurs is a function of the height of the aircraft over the ground and decreases as the height of the aircraft increases. As discussed in reference 1, another interesting phenomena is that of vortex rebound in which the viscous action between the ground and the vortex system causes the primary vortex to "bounce" upward after it has come close to the ground. Thus, one of the objectives of these experiments was to be able to distinguish between the phenomena of vortex rebound and the nearly identical results that would occur solely due to side wall effects. Unlike the case of vortex rebound, which occurs in the full-scale situation as well as in its modelling, in order for the ground deposition data to be valid, it is essential that the deposition test particles be on the ground before the influence of the tunnel wall effects become significant.

The flow visualization technique used in these studies for obtaining the time histories of the wake development and decay involves the use of a nearly two-dimensional kerosene smoke screen which is injected into the test section just before the model arrives. High-speed cameras are used to obtain a photographic record of the vortex system formation, transport, and decay. A high-speed clock is also photographed in this record such that the non-dimensional position, in semispans, of the vortex system downstream of the aircraft can be determined. From the high-speed movies, selected frames are chosen from which photographic prints are obtained. Examples of these prints are shown in figures 6 through 9, which depict the vortex system at 10, 30, 50, and 100 semispans downstream of the model, respectively. By placing a grid over photographs such as these, the non-dimensional trajectory of the cores of the trailing vortex system can be determined and plotted.

EXPERIMENTAL RESULTS AND DISCUSSION

Particle Deposition Experiments

The results of the baseline scaling law validation experiments are summarized in figures 10, 11, and 12. As previously outlined, the baseline configuration evolves a model height of 0.51 semispans (particle ejection height of 0.46 semispans), a lift coefficient of 0.61, and a scaled to full-size particle diameter of approximately 490 microns. Figure 10 pictorially represents a rear-view of the model in which the particle trajectory and the median ground deposition point from each of the ejectors are depicted. Thus, the physical interpretation of this figure is realized by observing, for example, that a particle ejected from the 0.6 semispan position is transported by the vortex system to 1.13 semispans at which ground deposition occurs. As can be noted in the figure, particles ejected outboard of approximately 0.25 semispans are transported outward by the tip vortex system, while particles ejected inboard of 0.25 semispans are transported inward by the wing-fuselage intersection vortex. Thus, a particle ejected near the 0.25 semispan location could not be laterally transported at all, but rather, would fall directly downward to its deposition point. It would also be expected that at the model centerline, the left and right vortex systems cancel, and a particle ejected from the lateral centerline should fall directly downward. This region where the left and right wing-fuselage intersection vortices interact is, however, extremely sensitive to any deviations in yaw angle or other model misalignments. This problem is manifested in these experiments in which the particles ejected from the model centerline are seen in figure 10 to be deposited 0.06 semispans to the right of centerline. It should be pointed out, however, that the quantity of data taken using the centerline ejector is quite limited

and available only for the 0.15 scale model. Therefore, any conclusions regarding the deposition behavior near the centerline must be restricted. The information that is depicted in figure 10 is presented more compactly, for all three model scales, in figure 11. In this figure, the difference between the median ground deposition point and the initial ejection point is indicated as the "lateral displacement of median" on the vertical axis. Thus a particle ejected from the 0.4 semispan ejector position, for example, is transported approximately 0.2 semispans outboard. The point where the curve crosses the horizontal axis, at about 0.25 semispans, corresponds to the point at which no lateral transport to an ejected particle occurs. Points above the horizontal axis are transported outboard, while points below are transported inboard. As in figure 10, the particles ejected from the centerline position, which should fall without lateral transport, are shown to be deposited at 0.06 semispans to the right (positive) of centerline. Because of the uncertainty resulting from the limited amount of data taken from the centerline ejector, the curve which connects the data obtained from the centerline and the 0.2 semispan ejector positions is shown as dashed in the figure.

The validity of the scaling laws is indicated in figure 11 by the excellent agreement shown between the data collected for the different model scales. Based on the close agreement shown in these cases, it can be surmised that if the scaling laws are used to determine the size and density of a particle to be used in an experiment which simulates the behavior of a full-scale 490 micron diameter water droplet, for example, then the experimental non-dimensional median deposition points should accurately correspond to the full-scale non-dimensional median deposition points.

Figures 12(a) through 12(f) compare the actual deposition patterns obtained from the ejectors at 0.2 semispans through 0.7 semispans for the different model scales. As expected, these figures demonstrate that the

concentration patterns are increasingly more spread out for the particles ejected from the more outboard locations because of the stronger influence of the tip vortex in these regions. Although the deposition patterns between the three model scales are quite similar, a fairly consistent difference is that the peak concentrations of the 0.10 scale model deposition patterns are somewhat lower, and the deposition pattern widths slightly wider, than are those of the two larger scale models. Part of the reason for the discrepancy is due to the fact that the 0.10 scale particle actually only scales to a 477 micron full-scale water droplet which allows the flowfield to have a slightly greater influence than it does on the particles which scale more closely to the 490 micron droplet. A further explanation is that the error introduced by small, random air motions, which are most likely nearly constant, is relatively much more significant for the small scale model than it is for the larger scale cases. Thus, it causes the 0.10 scale model deposition patterns to spread out compared to the larger model scale patterns, and consequently, the peak concentration values also decrease.

While only the mean particle characteristics were selected using the scaling laws, and no attempt was made to scale the actual deposition patterns, the close agreement that is found between the patterns obtained from the different model scales suggests that the deviations from the mean particle characteristics for the different model scales must be relatively uniform. Thus, for future testing, it should be possible to adjust the variation in model particle characteristics to be in agreement with full-scale droplet variations such that similar deposition patterns between the two are obtained.

Figure 13 presents, in addition to the baseline data obtained for a lift coefficient of 0.61, data collected for the case of a lift coefficient of 0.48. As expected, in the region of outward particle transport, operation of the model at a lower lift coefficient decreases the amount of lateral transport

with the influence increasing as the ejector location moves outboard. In the region of inboard transport, although the data is again limited, it is difficult to observe a significant effect due to the variation in operational lift coefficient. From this figure, as well as the combined deposition patterns for particles ejected from the 0.3 and the 0.6 semispan ejectors, shown in figure 14, the use of the scaling laws to properly size the experimental particles provide consistent results for the 0.10 and 0.15 scale models at a lift coefficient of other than the baseline.

In order to ascertain the effect on the median particle deposition points due to height variation away from the baseline value, data were obtained for the 0.10 and the 0.15 scale models at a height of 0.35 semispans. These data are presented along with the baseline configuration data for comparison in figure 15. The combined deposition patterns for the 0.3 and the 0.6 ejector positions are presented for the model height of 0.35 semispans in figure 16. Qualitatively, operation of the aircraft closer to the ground allows less lateral transport to occur than when the aircraft operates at higher altitudes. Again, the use of the scaling laws in sizing the particles for these experiments results in excellent non-dimensionalized agreement between the 0.10 and the 0.15 scale models.

In order to examine the sensitivity of the deposition experiments to the size of the particules utilized, tests were run in which the particles used did not scale to a common full scale droplet. The results of these tests are given in figure 17. The importance of properly scaling experimental particles can be realized by the significant shifts that occur in the deposition median when the particle is scaled from the baseline 490 micron droplet, to either a 390 micron droplet, or a 580 micron droplet. This effect can be further realized by noting the combined deposition patterns for the 0.3 and the 0.6 ejector positions as shown in figure 18.

In order to be certain that the excellent agreement between the three model scales which resulted from using the scaling laws to size the particles was not coincidental to the full-scale 490 micron droplet, an independent validation was performed by ejecting a scaled 200 micron droplet from the 0.4 ejector position for the 0.10 and the 0.15 scale models. Although these tests were performed at a model height of 0.35 semispans, the results are included in figure 17 along with the other results for varying the particle scale which were obtained using a 0.51 semispans model height. From the close agreement of these points, along with the combined deposition patterns for this case shown in figure 19, the use of the scaling laws has again provided excellent agreement between the two model scales.

The results of preliminary propeller-on baseline median deposition points are presented in a manner to facilitate physical interpretation in figure 20. It must be emphasized that only a minimum number of runs were made in obtaining the prop-on data. Therefore, these results should be regarded primarily to provide guidance for future prop-on research. As shown in figure 20, the direction of propeller rotation, when viewed from the rear of the model, is clockwise such that a right-hand helical flow-field is induced. This results in the rightward shifting of the more inboard particle trajectories. The same data of figure 20 are presented for the 0.10 and the 0.15 scale models in figure 21. In this case, both the port (left) and starboard (right) sides are depicted. Also included in this figure are the baseline prop-off data for comparison. The dashed line represents the starboard (positive) side data for the model and, as such, the axes scales correspond to positive values. Thus, a particle ejected from the centerline is deposited at about 0.16 semispans on the starboard side. The dotted line, on the other hand, represents the port (negative) side, and the scales indicate negative quantities. In this case, a particle ejected from the centerline is transported to the oppo-

site (starboard) side and is therefore indicated at a negative 0.16 semispans.

The upward shift of the prop-on deposition medians shown in figure 21 over that of the prop-off data is thought to be due to the unstable pitch contribution of the propeller that causes the model angle of attack to be greater than that which was set with the model at rest. Hence, the prop-on data is obtained with a lift coefficient greater than that of the baseline configuration and a value of 0.75 is estimated. Consequently, the results of the prop-on experiments exhibit an increased amount of lateral transport over those results obtained for the prop-off case.

The agreement between the 0.10 and the 0.15 scale prop-on model configurations for the region between the centerline and the 0.3 semispan ejector positions is not nearly as good as it is in any of the preceding cases. With the limited amount of information available for this region, any conclusions must be considered tentative; however, it is possible that the discrepancies between the results for the two model scales are due to Reynolds number differences in the sensitive region where the propeller slipstream is interacting with the fuselage and the wing-fuselage intersection. Certainly a more detailed study of the region is necessary before extensive prop-on experiments are undertaken.

With the exception of the uniformly upward shift of the deposition medians as previously noted, the data shown in figure 21 indicate that the propeller has very little effect on the deposition median of particles ejected outboard of 0.3 semispans. This conclusion is further substantiated by the lack of assymmetry found between the deposition patterns from the -0.3 and the +0.3 semispan ejectors shown in figures 22(a) and 22(b).

Vortex Trajectory Experiments

The first phase in determining the test envelope for the NASA/Langley Vortex Research Facility was a theoretical analysis which was performed using the computer programs developed in reference 2. The results of this study are presented in figures 23 and 24. These plots can be used to determine for what model test conditions an ejected particle will land on the ground before the flowfield becomes distorted due to side wall effects. Both figures consider model spans of 1.22, 1.83, and 2.44 meters, and scaled to full-size particles diameters of 100, 200, and 500 microns. Figure 23 considers the effect of varying model height, while figure 24 examines varying lift coefficient. The straight horizontal lines in the figures indicate the maximum distance downstream from the model for which the wake in the tunnel has the same characteristics as the wake in free air. For example, on figure 24 for a lift coefficient of 0.540 and the 1.22 m span model, the wake is unaffected by the tunnel walls for the period of time required by the model to travel some 64 semispans down the tunnel from the point at which wake formation occurs. The distance downstream for which the flowfield is valid for each case was determined using the inviscid vortex trajectory computer code based on the method described in reference 2 and incorporating the tunnel walls. Those calculations were compared to free air calculations and the downstream distance where the two trajectories diverge, that is, where the vortex path in the tunnel begins to turn upward and climb the wall, is noted as the point where the flowfield in the tunnel becomes distorted. The curved lines in the figures indicate the distance downstream that a certain size particle lands when it is ejected in free air, with no initial velocity, from a given spanwise location.

As an example of the use of these plots, consider, on figure 24, the case of a model having a span of 1.83 m, a lift coefficient of 0.713, and

the release of a scaled 100 micron diameter particle. For this example, it is seen that the flowfield is valid up to approximately 23 semispans downstream. If the particle is ejected from the 0.1 semispan location (horizontal scale), it will land in free air approximately 26 semispans downstream (vertical scale). As this is further downstream than the flowfield is valid, such a test would be out of the facility envelope. Note, however, that for this same case, a particle ejected from 0.4 semispans lands approximately 16 semispans downstream and is, therefore, within bounds of the test facility envelope.

The generality of figures 23 and 24 for designing particle dispersal experiments can be extended somewhat if it is pointed out that the curves shown are actually based on a non-dimensional circulation strength

$$\overline{\Gamma} = \frac{\Gamma}{U_\infty b} = \frac{C_L}{AR}$$

where

$$\Gamma = \frac{C_L U_\infty b}{AR}$$

Thus, the curves indicated in figures 23 and 24 hold true for any experiment in which the ratio of the lift coefficient to the aspect ratio can be made equal to any of the cases indicated.

Typical experimental vortex trajectories for each of the three models described previously are shown in figures 25, 26, and 27 in which the vertical position of the vortex core is plotted vs. its distance from the test section centerline. These plots were obtained from photographic sequences similar to the examples shown in figures 6 through 9 and discussed previously. The model speeds indicated on the trajectory plots all scale to a full-size aircraft of 12.2 m (40 ft) span and having a flight speed of 53.3 m/sec (175 ft/sec). Also noted on the two-dimensional vortex trajectories is the distance traveled by the model, in semispans, down the tunnel from the point at which the trajectory initiated. Thus, the figures pictorialize a front view of a portion

of the test section in which the vortex is shed from the wingtip near the left-most point shown and is transported outwardly (to the right) toward the test section wall. The slight rebound of the trajectory at about 1.4 semispans from the centerline is thought to be caused by the vortex bounce phenomena. The side wall influence is seen to be somewhat more dramatic and begins at shorter distances downstream for the larger model. In the case of the smallest span model (1.22 m), it is difficult to accurately define the point at which the side wall interference becomes significant because as the vortex weakens due to viscous dissipation, the core tends to wander; however, the core is clearly seen to climb the wall somewhere between 72 and 90 semispans downstream of the model. Interpolation using the theoretical results in figures 23 and 24 indicate that the flowfield becomes invalid due to the wall interference at approximately 95 semispans downstream. The point at which wall interference occurs for the cases using the two larger models can be obtained by comparing their vortex trajectories, figures 26 and 27, with that of the smaller model, in which the wall effect is felt relatively far downstream, and noting the point at which the trajectories diverge. In this manner, the vortex from the 1.83 m span model was found to be influenced by the test section wall at about 52 semispans downstream; and, for the case of the 2.44 m model, the vortex bounce phenomena seems to be lost in the wall effect which was found to occur at approximately 28 semispans downstream. These experimentally determined downstream distances for which wall effects are observed are in very good agreement with those determined by interpolation from the theoretical results, figures 23 and 24, and found to be 54 and 25 semispans downstream respectively. Thus, it seems reasonable to conclude, on the bases of these experiments, that the theoretically developed facility test envelope can provide reasonable estimates in establishing the boundaries of particle dispersal experiments.

One further result which is worthy of examination involves the intuitive

notion that, except for the relatively small differences in the size of the vortices shed from the three models in these experiments, it seems plausible that the influence of the wall should occur when the vortex core is at approximately the same physical distance away from it. This assumption is somewhat justified by the experimental results from which it is found that for all three model sizes, the wall influence becomes significant when the vortex core reaches a position approximately 1.47 m ($\pm$ 0.15 m) from the test section wall.

CONCLUSIONS AND RECOMMENDATIONS

Based on the experimental results of this research program, it is clear that the particle scaling laws, as developed in reference 3, provide a proper scaling of the relationship between the particle dynamics and the flowfield as is necessary for the study of particle dispersal in the wake of agricultural aircraft of different sizes. The use of the scaling laws to establish the test parameters for experiments covering a wide range of possible conditions provided significant agreement between the results of commonly scaled tests. It is recommended, however, that further studies be performed on the region influenced by the wing-fuselage intersection in order to determine if effects due to model Reynolds number variations are significant. Furthermore, before extensive prop-on developmental experiments are undertaken, additional work is necessary in order to more accurately quantify the effect of the propeller slipstream on the particle deposition patterns.

The theoretical test envelope that has been developed for the Langley Vortex Research Facility was found to be consistent with an experimental investigation examining the influence of the tunnel walls on the flowfield behind an aircraft. If reasonable margins for error are maintained, the theoretical envelope should be a valuable guide in the establishment of the model testing parameters which can be accommodated by the facility.

In addition to the verification of the particle scaling laws, the experimental procedures developed during this program should provide the basic techniques necessary for future research examining particle dispersal behind agricultural aircraft.

REFERENCES

1. Jordan, F.L., McLemore, H.C., and Bragg, M.B., "Status of Aerial Applications Research in the Langley Vortex Research Facility and the Langley Full Scale Wind Tunnel", AIAA Paper 78-1481, August 1978.

2. Bragg, M.D., "The Trajectory of a Liquid Droplet Injected into the Wake of an Aircraft in Ground Effect", Aeronautical and Astronautical Engineering Department, University of Illinois, Technical Report 77-7, UIUC-ENG 770507, May 1977.

3. Ormsbee, A.I., and Bragg, M.B., "Trajectory Scaling Laws for a Particle Injected into the Wake of an Aircraft", Institute of Aviation, Aviation Research Laboratory, University of Illinois, Report ARL-78-1, June 1978.

4. Woan, C.J., "The Design of Propellers for Minimum Noise", Aeronautical and Astronautical Engineering Department, University of Illinois, Technical Report 77-13, July 1977.

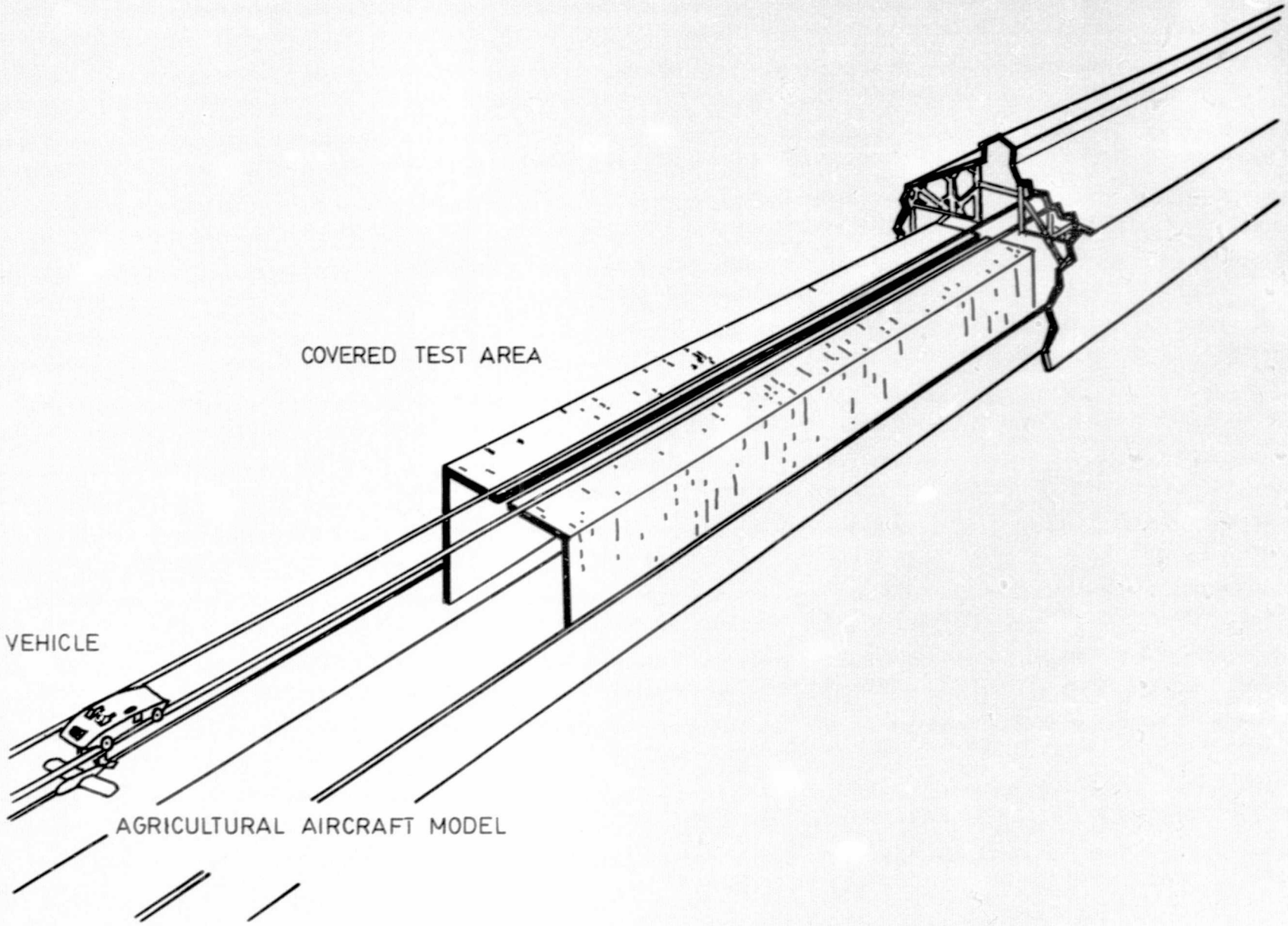

Figure 1. NASA-Langley Vortex Research Facility

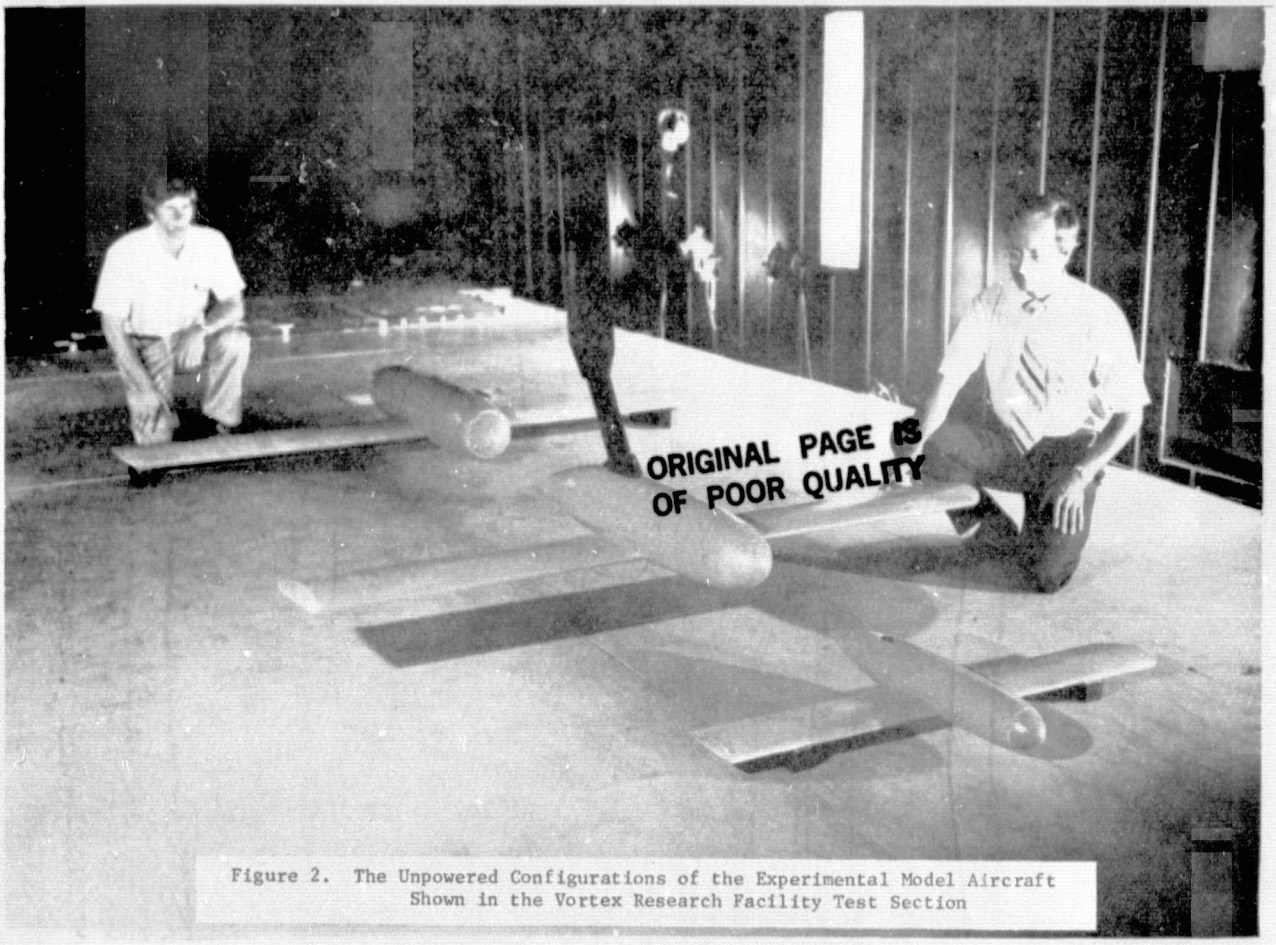

Figure 2. The Unpowered Configurations of the Experimental Model Aircraft Shown in the Vortex Research Facility Test Section

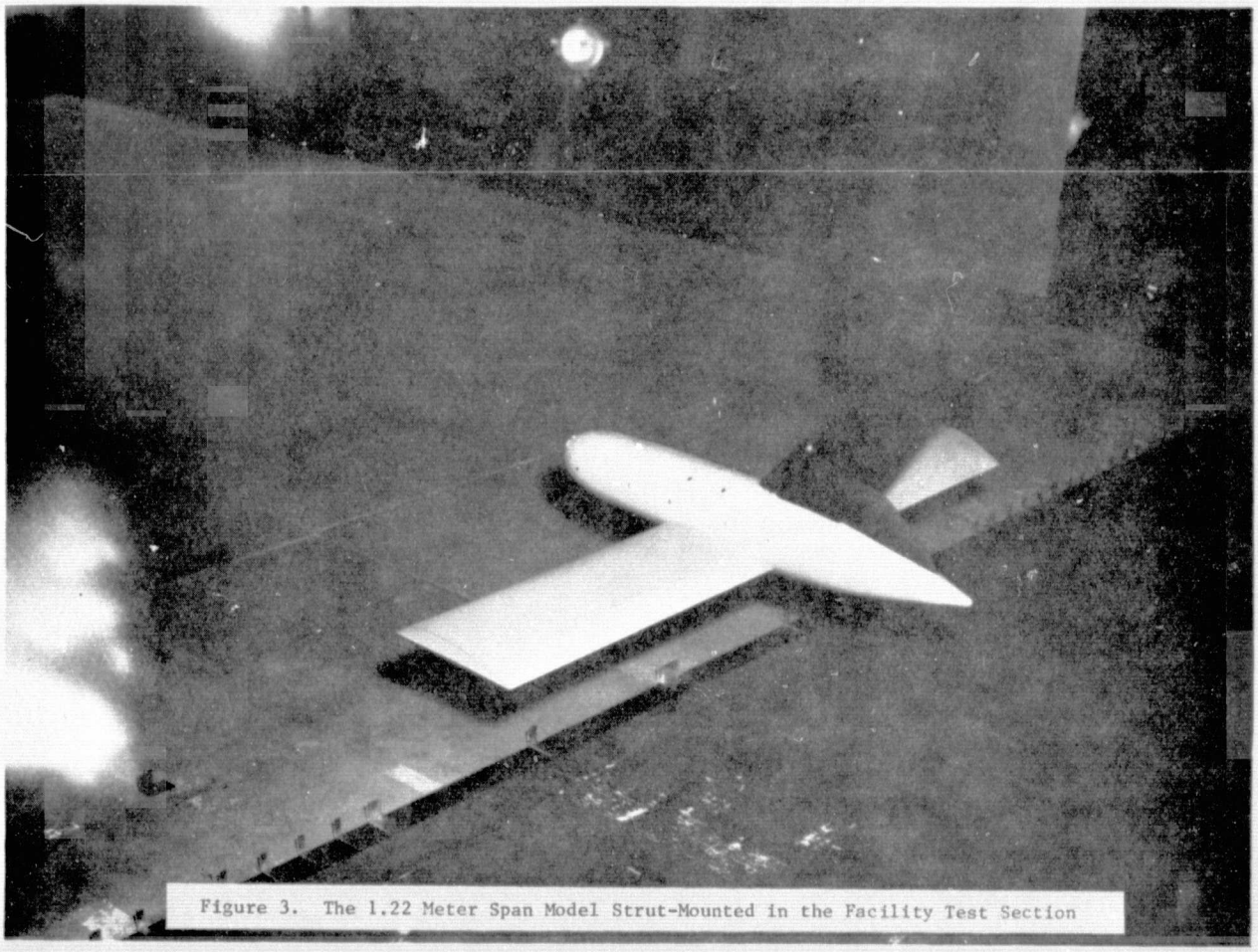

Figure 3. The 1.22 Meter Span Model Strut-Mounted in the Facility Test Section

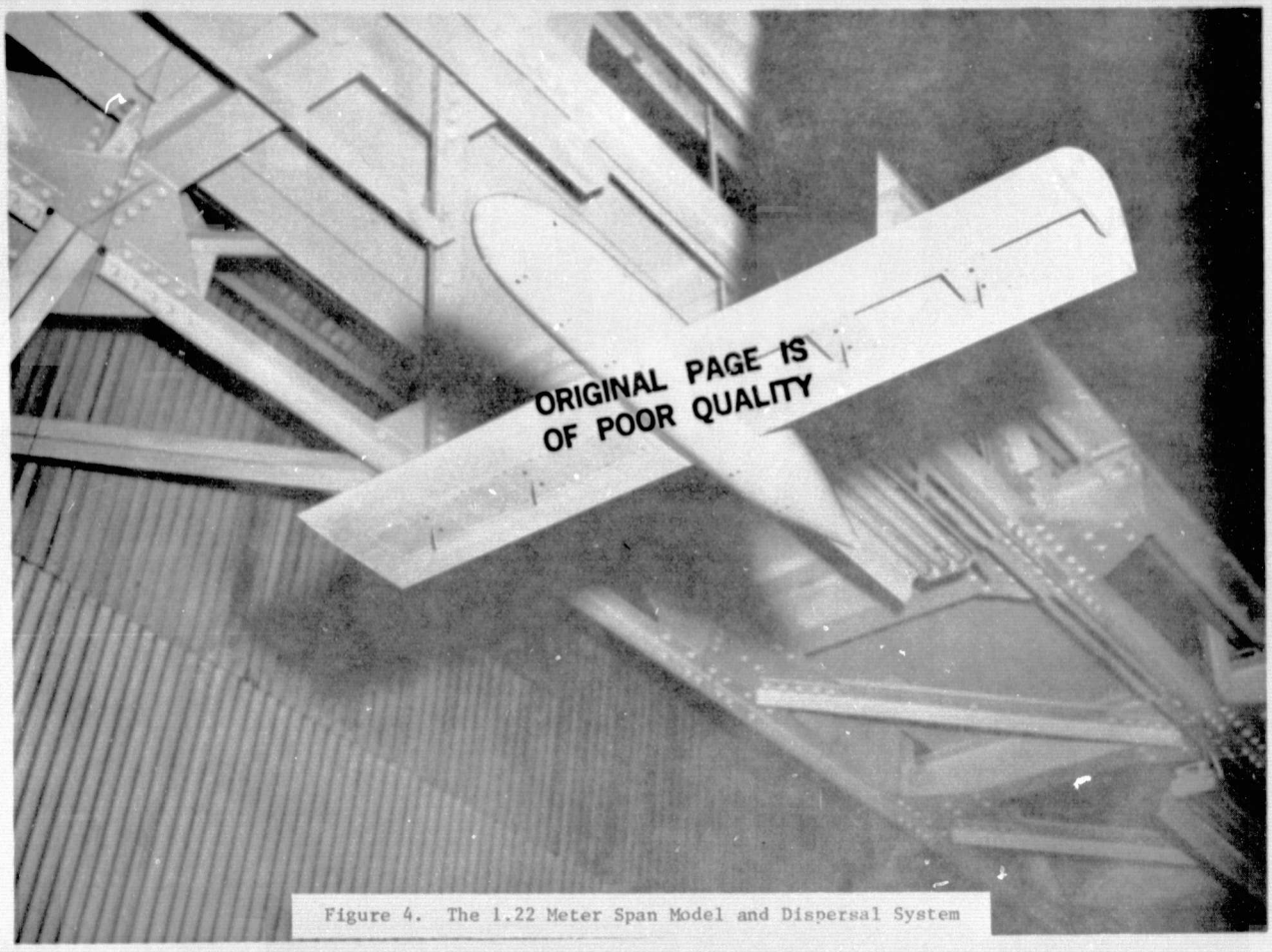

Figure 4. The 1.22 Meter Span Model and Dispersal System

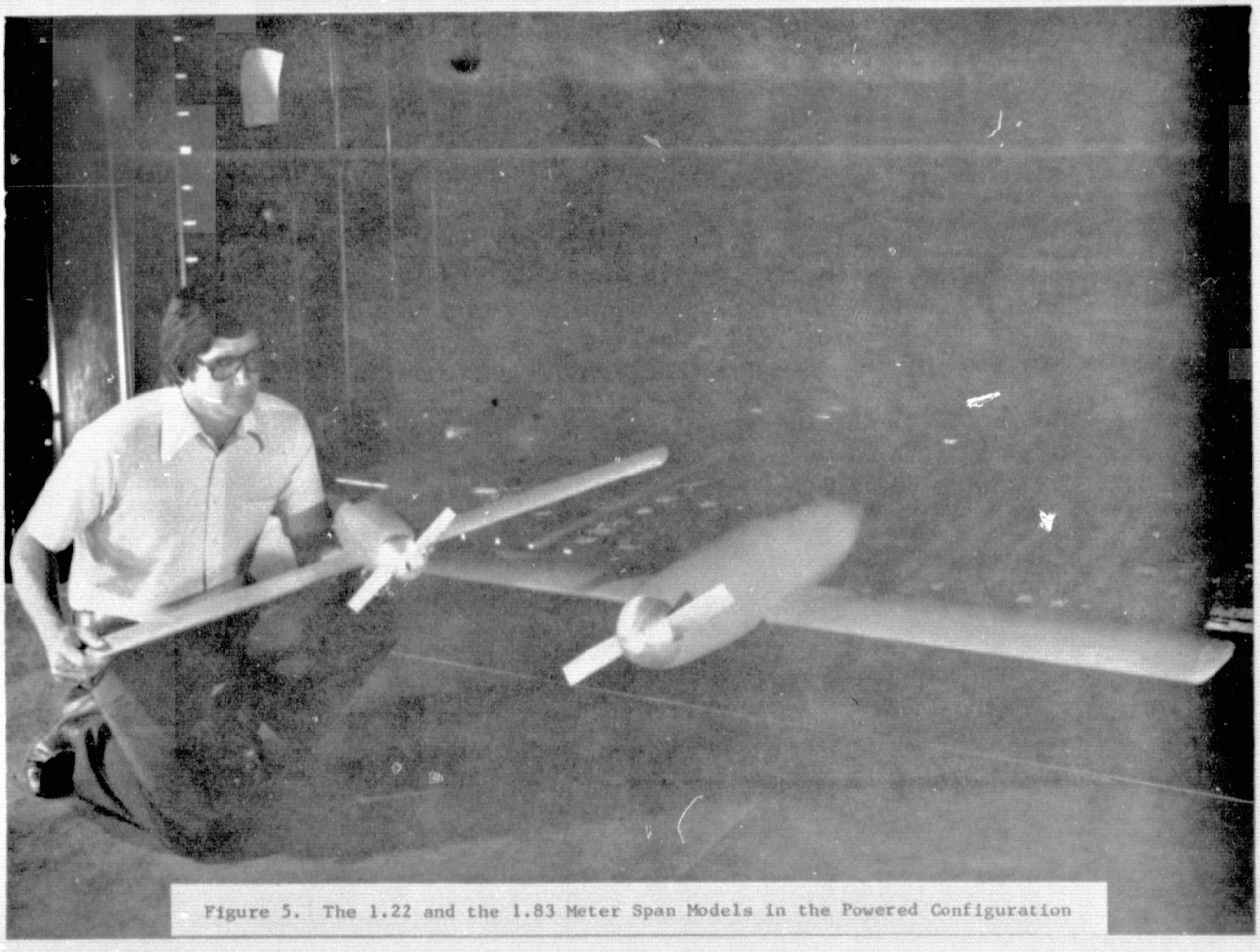

Figure 5. The 1.22 and the 1.83 Meter Span Models in the Powered Configuration

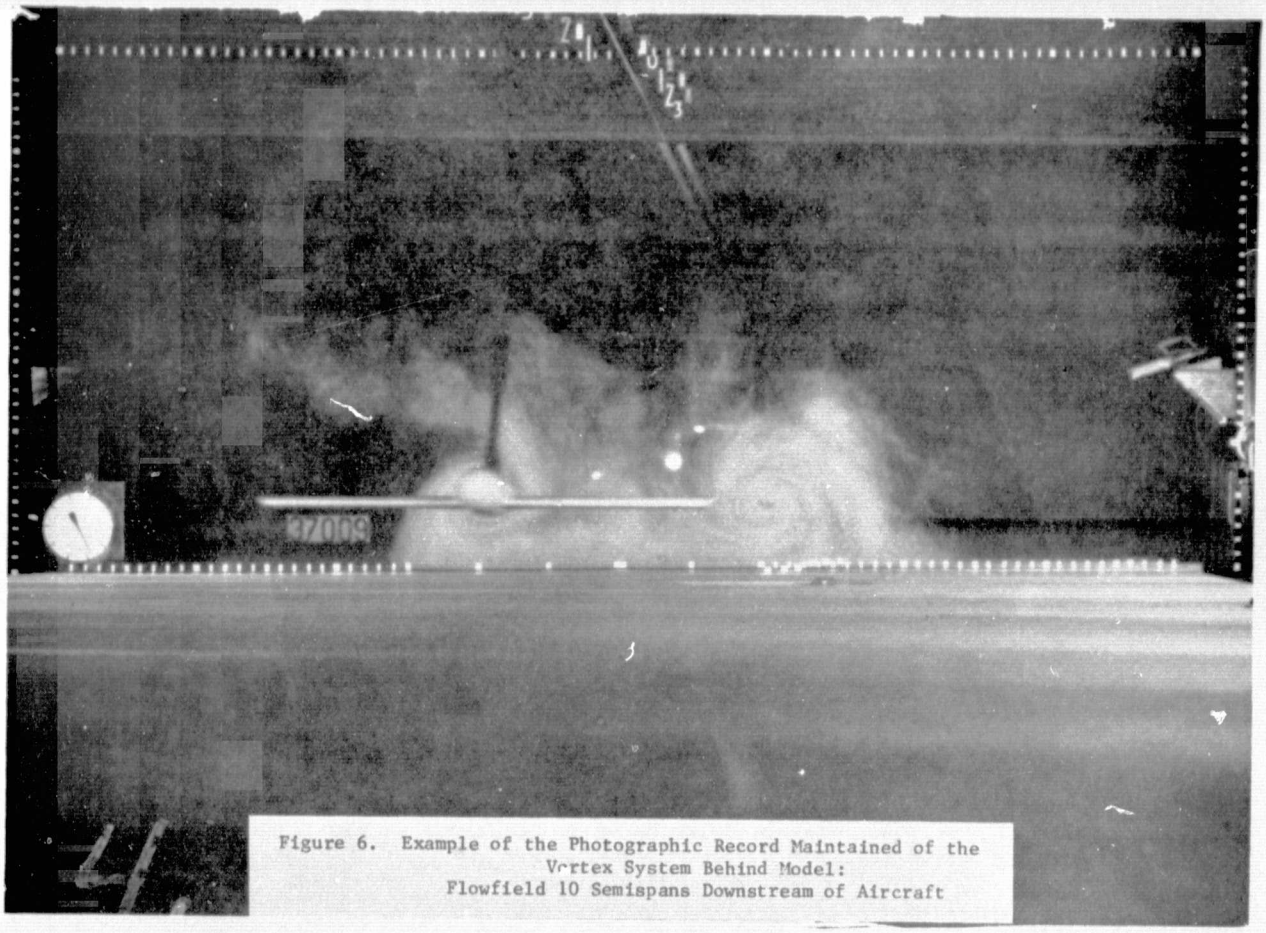

Figure 6. Example of the Photographic Record Maintained of the Vortex System Behind Model: Flowfield 10 Semispans Downstream of Aircraft

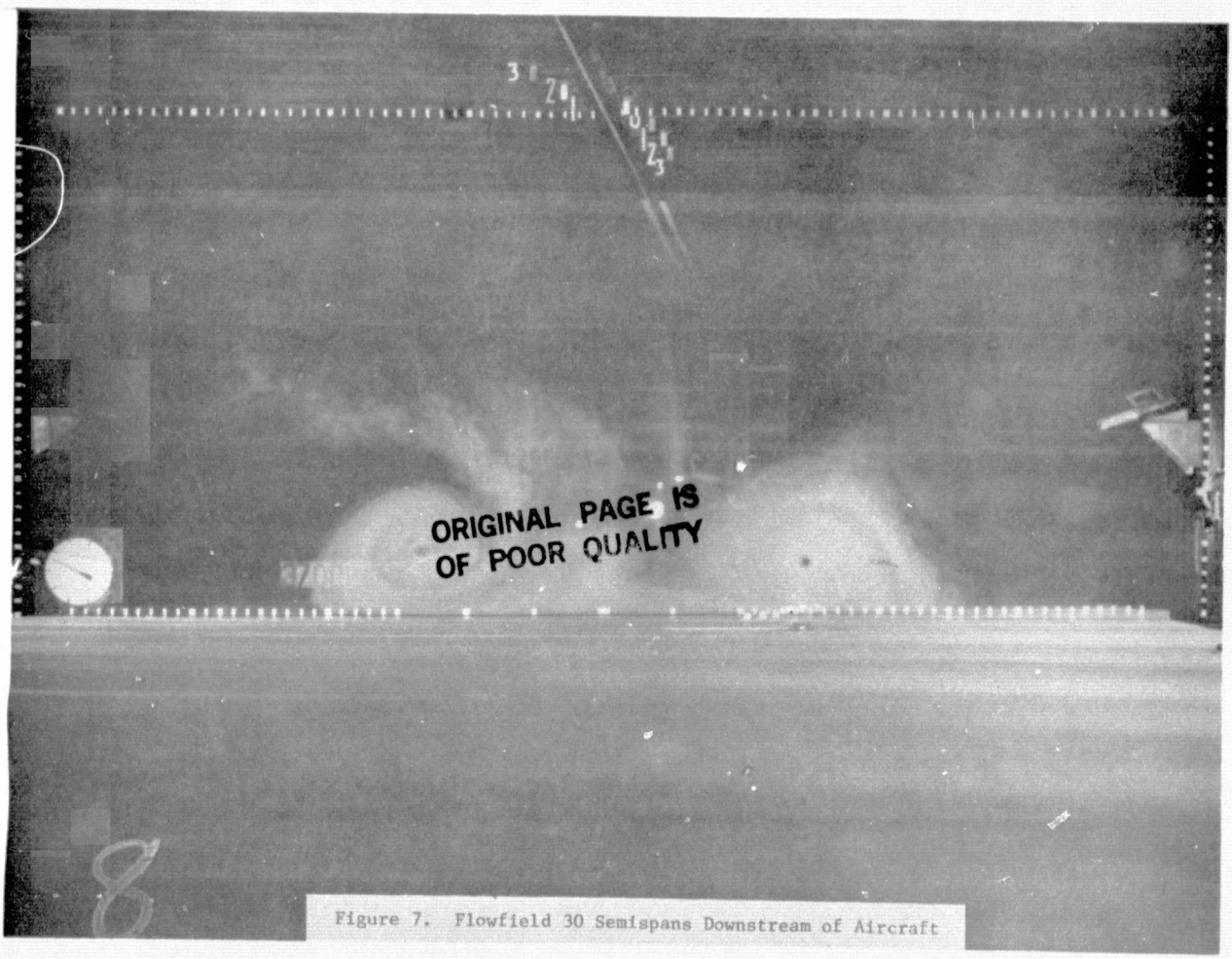

Figure 7. Flowfield 30 Semispans Downstream of Aircraft

Figure 8. Flowfield 50 Semispans Downstream of Aircraft

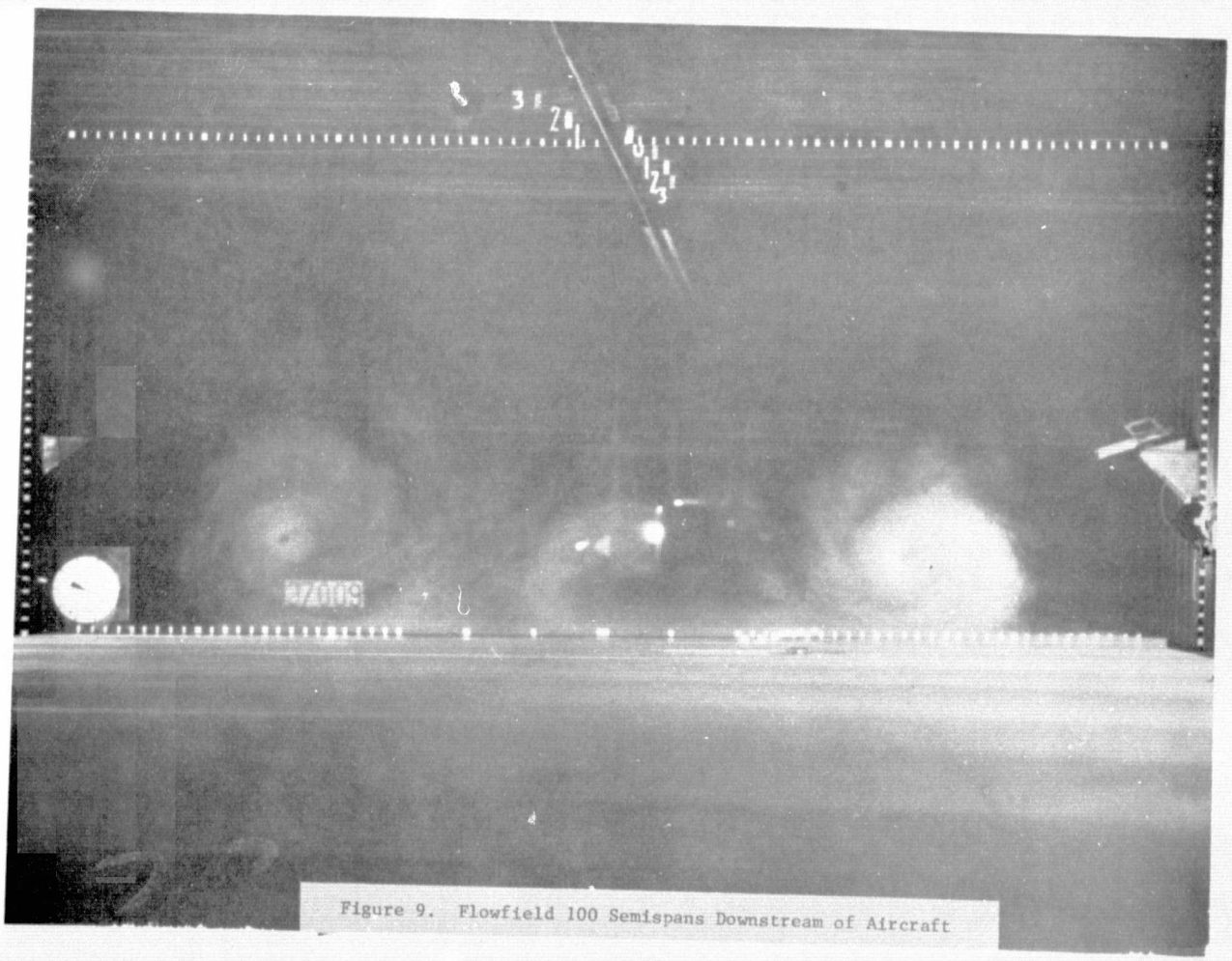

Figure 9. Flowfield 100 Semispans Downstream of Aircraft

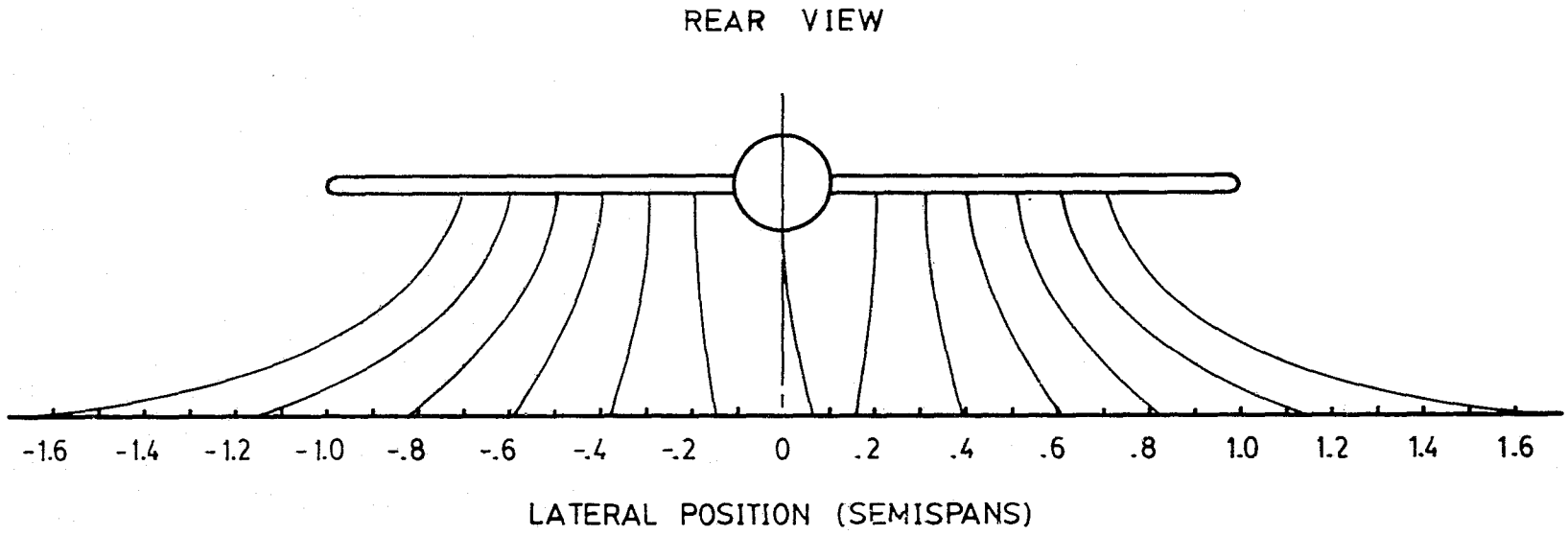

Figure 10. Median Deposition Trajectories for the Prop-off Baseline Scaling Law Validation Experiments. H = 0.51 (Semispans), C_L = 0.61, Particle Size = 490 (Microns)

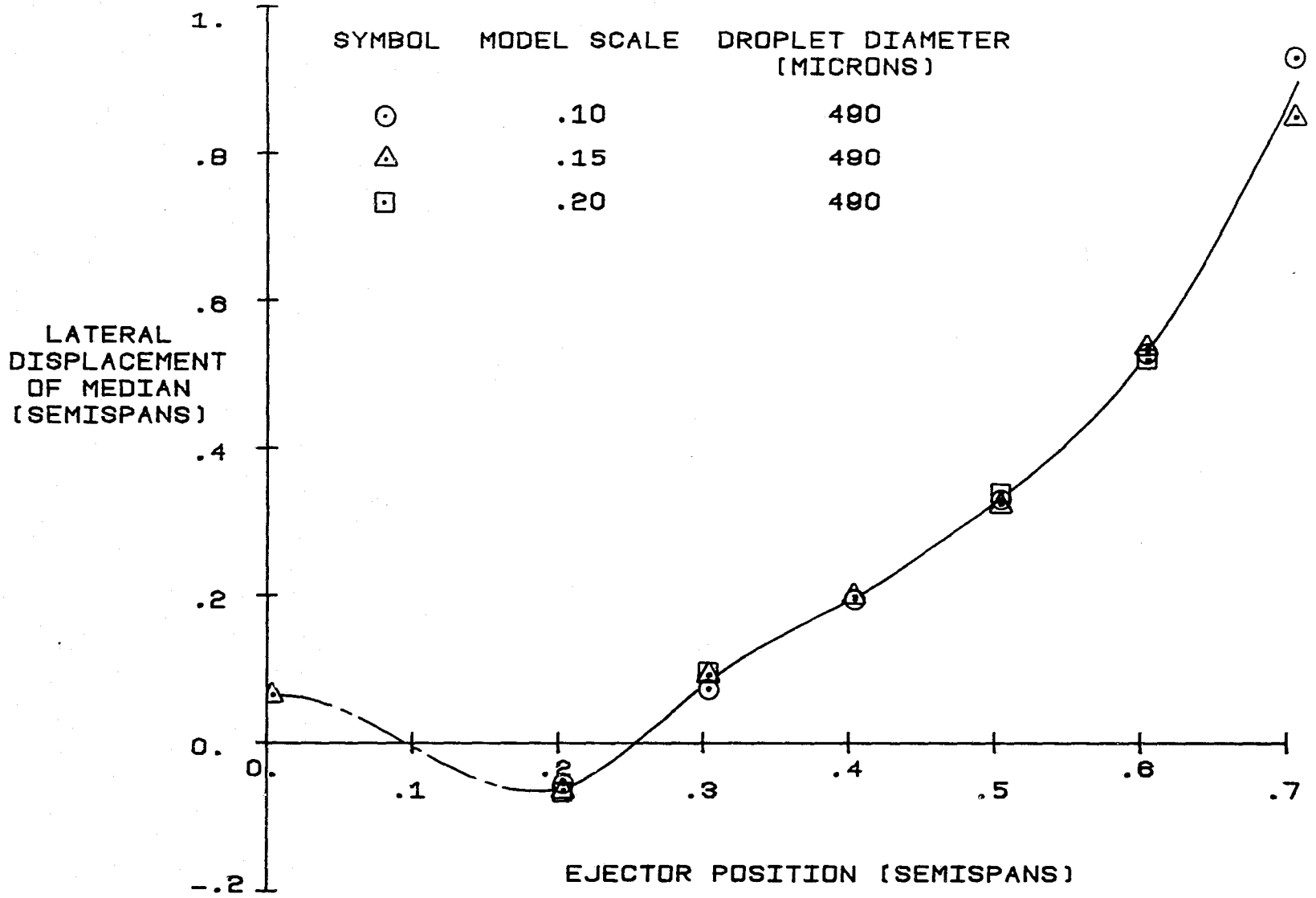

Figure 11. Lateral Displacement of Deposition Median as a Function of the Ejector Position for the Baseline Scaling Law Validation Experiments. H = 0.51 (Semispans), C_L = 0.61

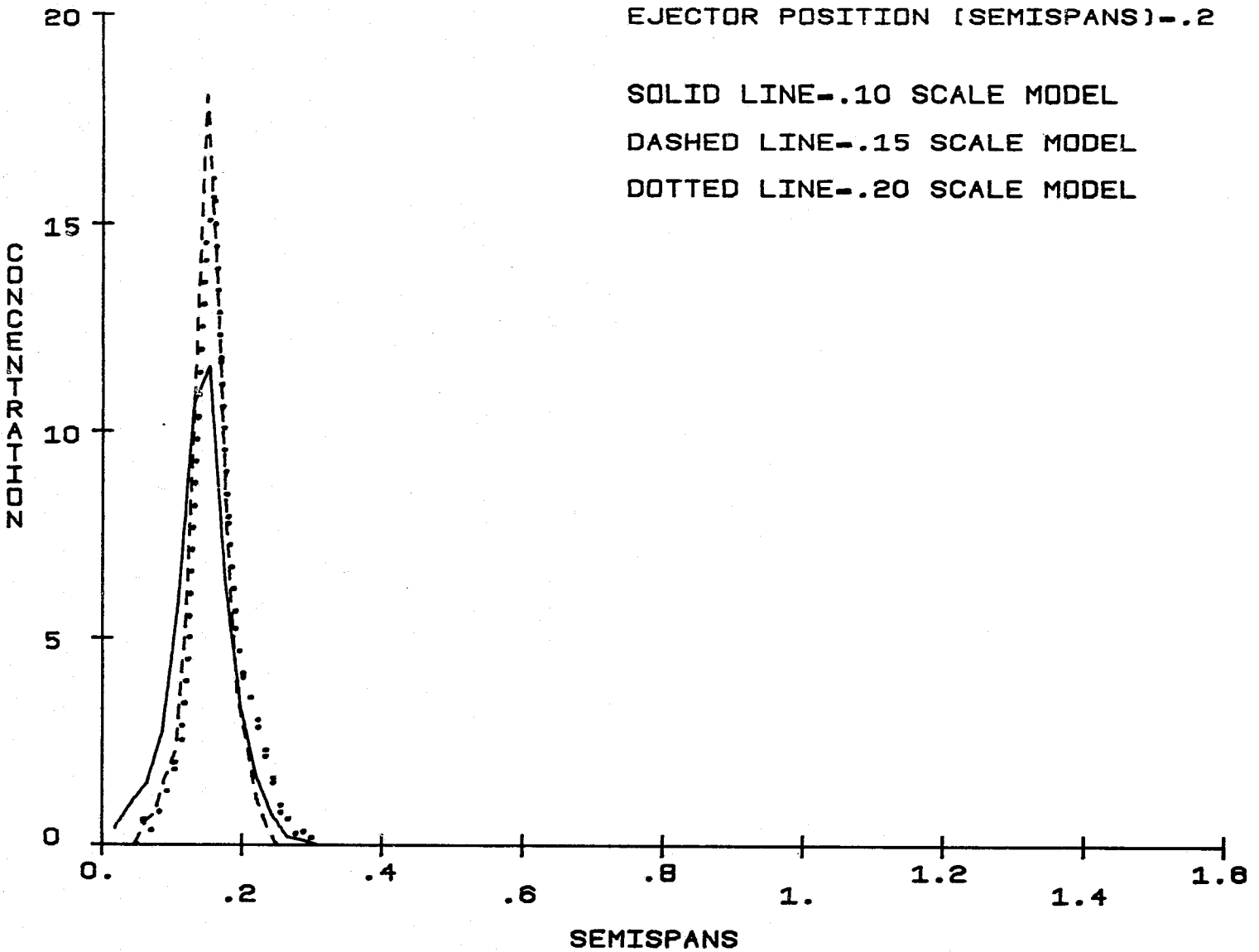

Figure 12(a). Deposition Patterns for the Baseline Scaling Law Validation Experiments. H = 0.51 (Semispans), C_L = 0.61, Particle Size = 490 (Microns)

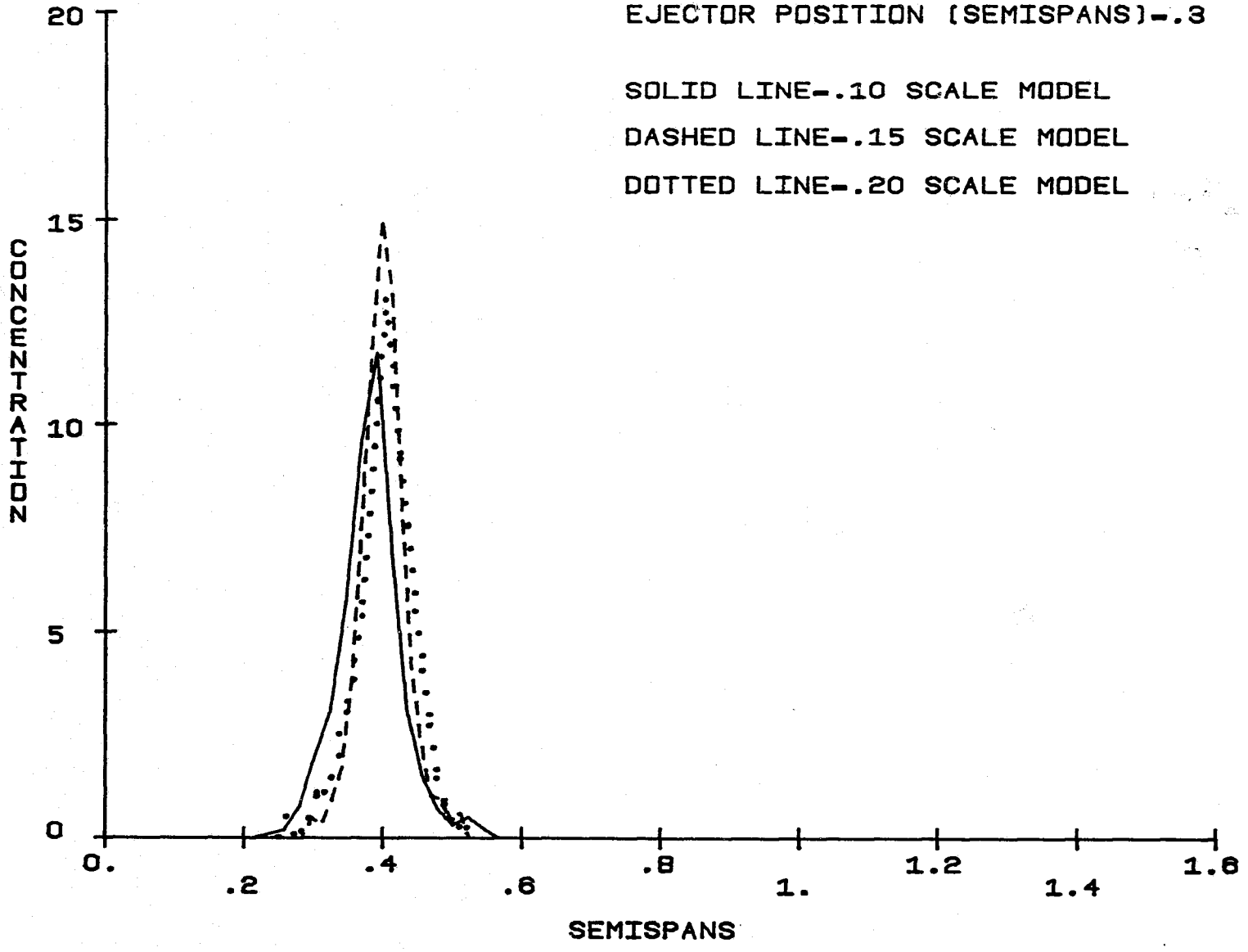
EJECTOR POSITION (SEMISPANS)=.3
SOLID LINE=.10 SCALE MODEL
DASHED LINE=.15 SCALE MODEL
DOTTED LINE=.20 SCALE MODEL
CONCENTRATION
20
15
10
5
0
0.
.2
.4
.6
.8
1.
1.2
1.4
1.6
SEMISPANS

Figure 12(b).

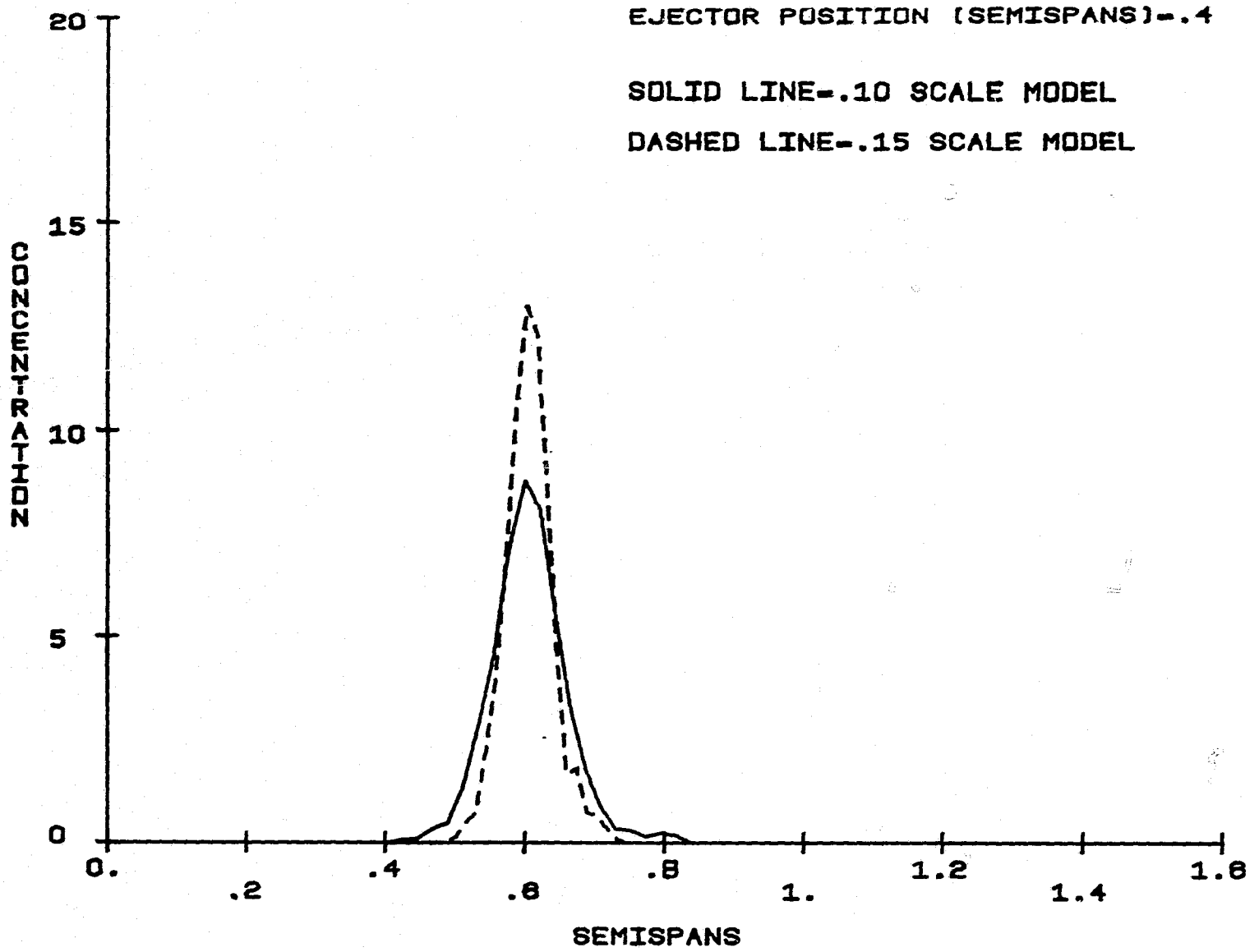
EJECTOR POSITION (SEMISPANS)=.4
SOLID LINE=.10 SCALE MODEL
DASHED LINE=.15 SCALE MODEL
CONCENTRATION
20
15
10
5
0
0.
.2
.4
.6
.8
1.
1.2
1.4
1.6
SEMISPANS

Figure 12(c).

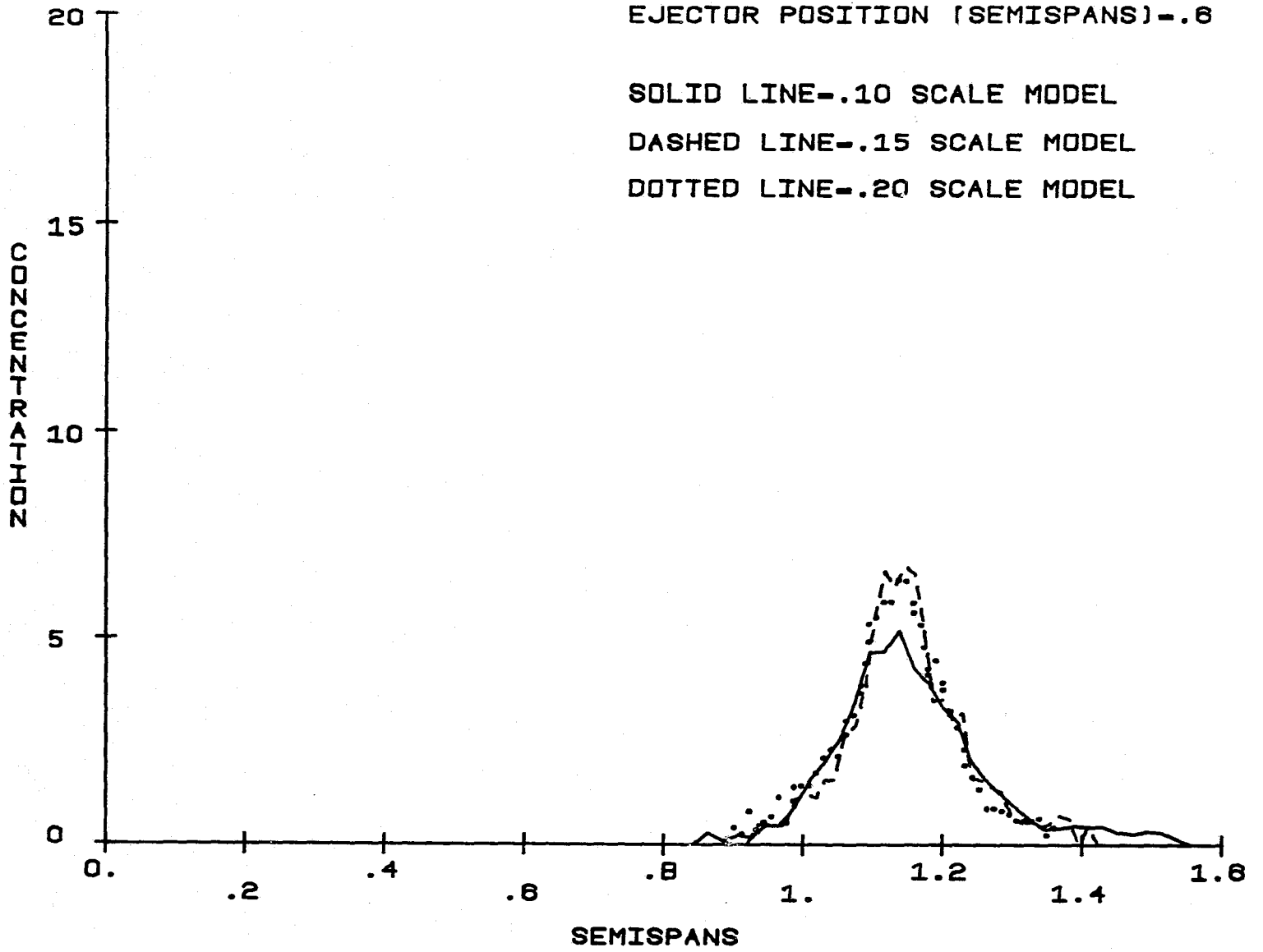
EJECTOR POSITION (SEMISPANS)=.6
SOLID LINE=.10 SCALE MODEL
DASHED LINE=.15 SCALE MODEL
DOTTED LINE=.20 SCALE MODEL
CONCENTRATION
20
15
10
5
0
0.
.2
.4
.6
.8
1.
1.2
1.4
1.6
SEMISPANS

Figure 12(e).

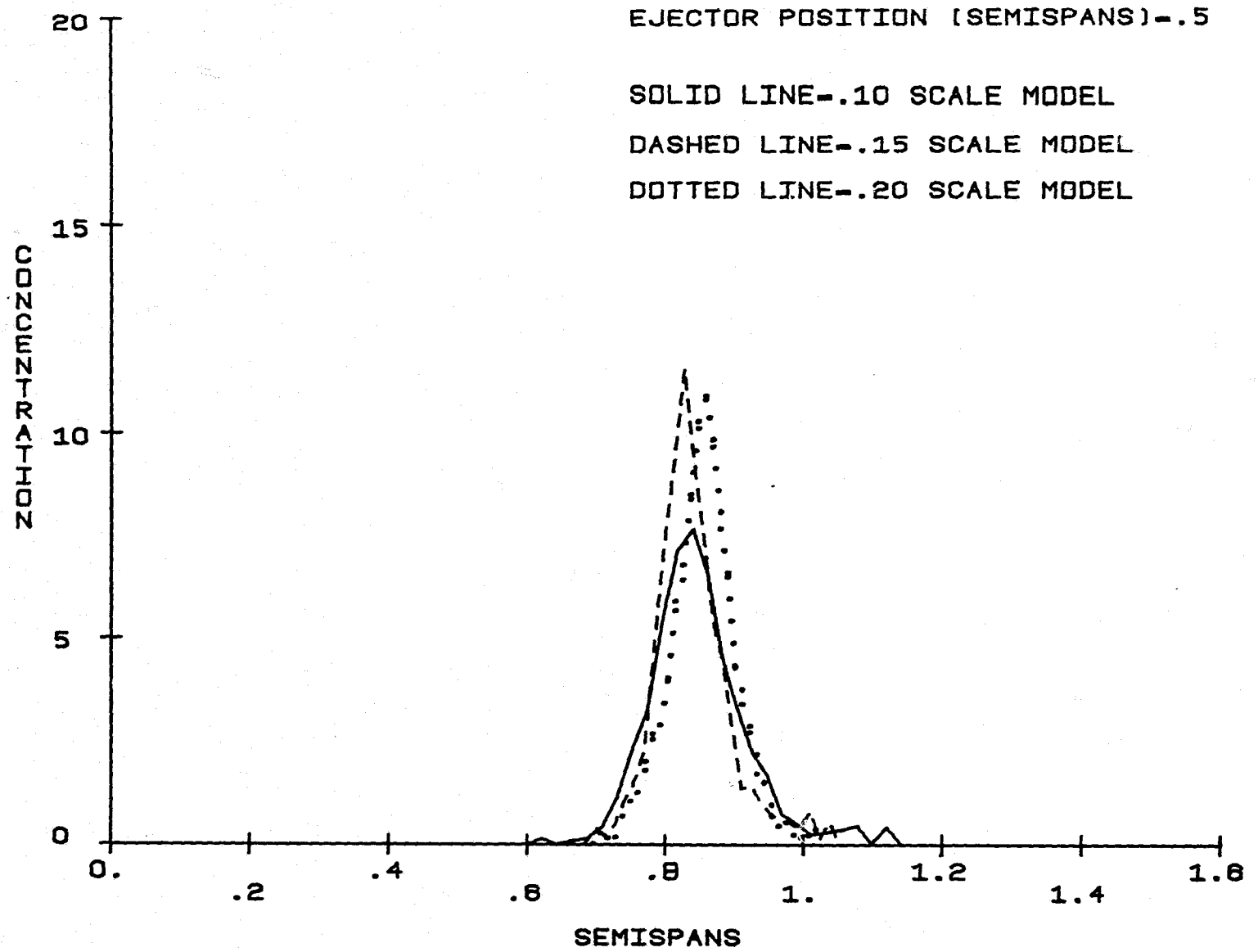
EJECTOR POSITION (SEMISPANS)=.5
SOLID LINE=.10 SCALE MODEL
DASHED LINE=.15 SCALE MODEL
DOTTED LINE=.20 SCALE MODEL
CONCENTRATION
20
15
10
5
0
0.
.2
.4
.6
.8
1.
1.2
1.4
1.6
SEMISPANS

Figure 12(d).

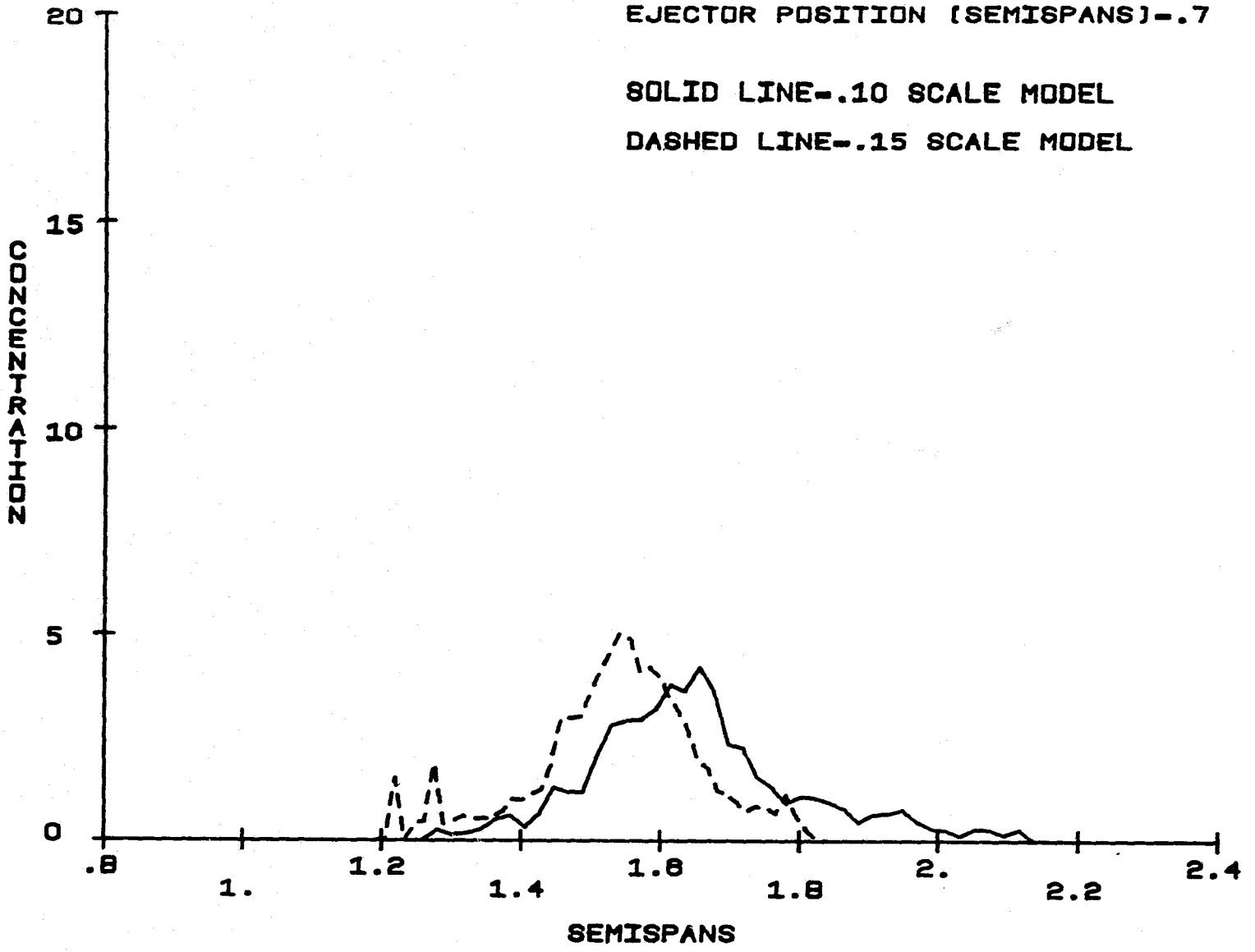

Figure 12(f). (Note shifted scale on horizontal axis)

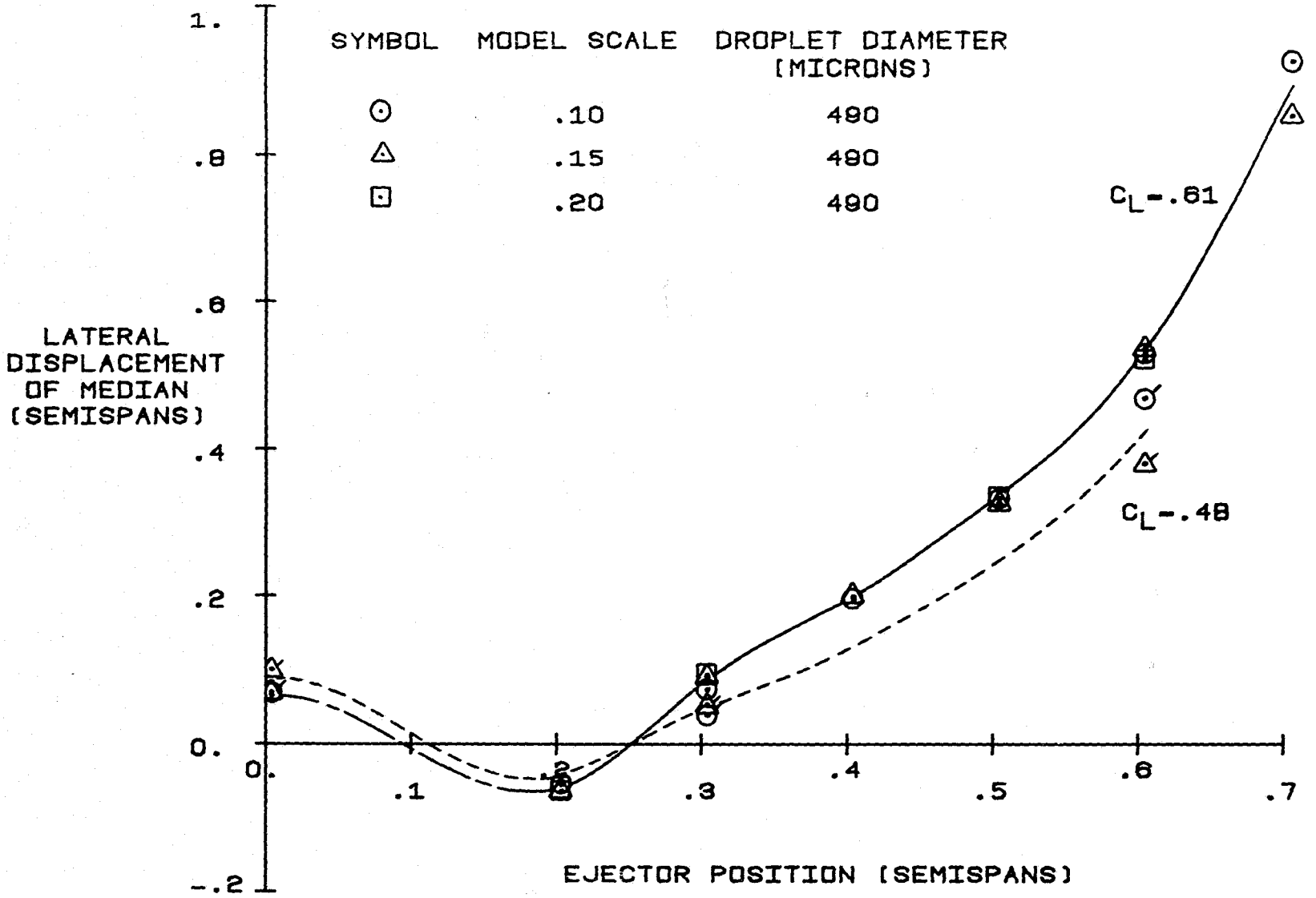

Figure 13. Lateral Displacement of the Deposition Median as a Function of the Ejector Position for Varying Lift Coefficients. H = 0.51 (Semispans), Particle Size = 490 (Microns)

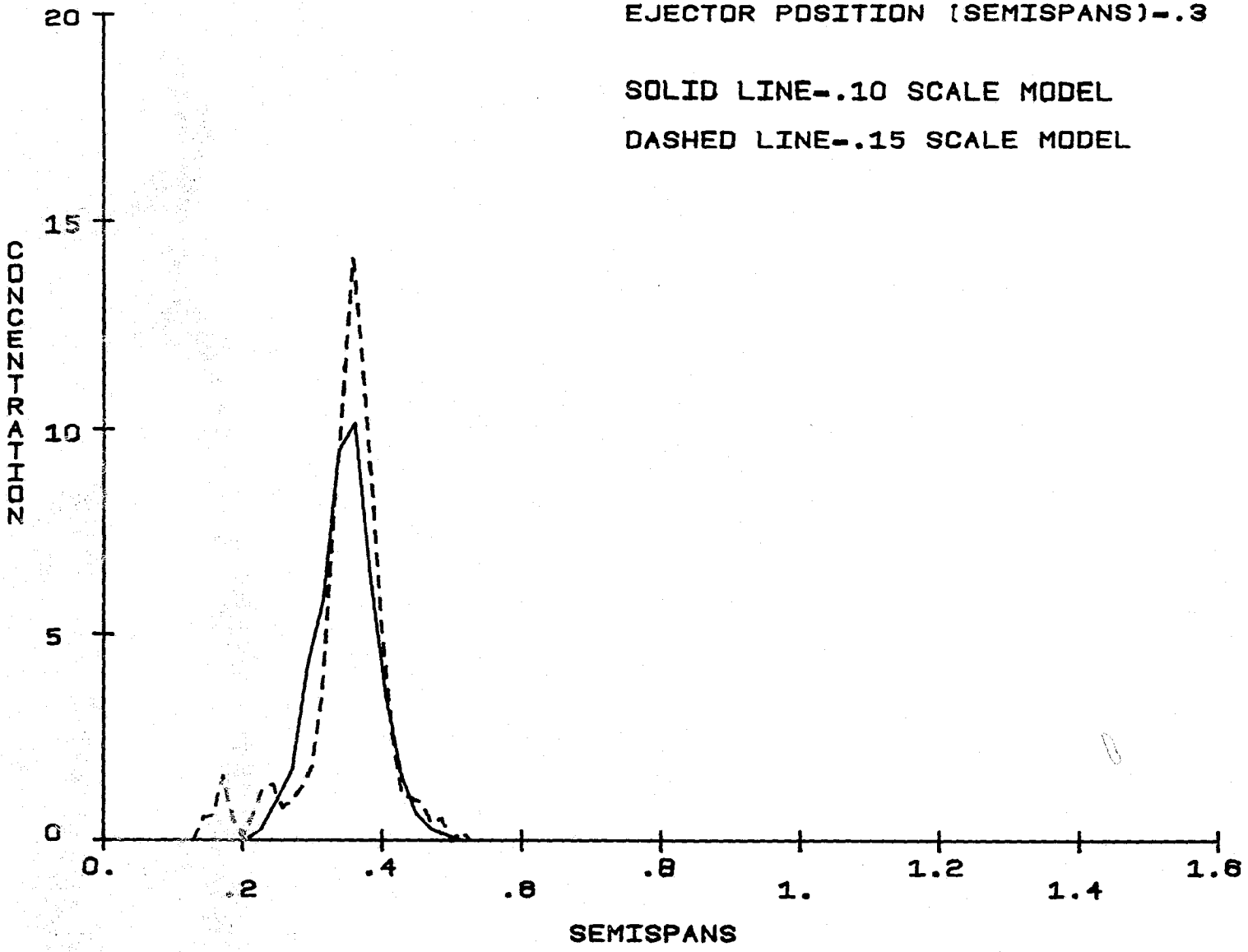

Figure 14(a). Deposition Patterns for the Scaling Law Validation Experiments with C_L = 0.48, H = 0.51 (Semispans), Particle Size = 490 (Microns)

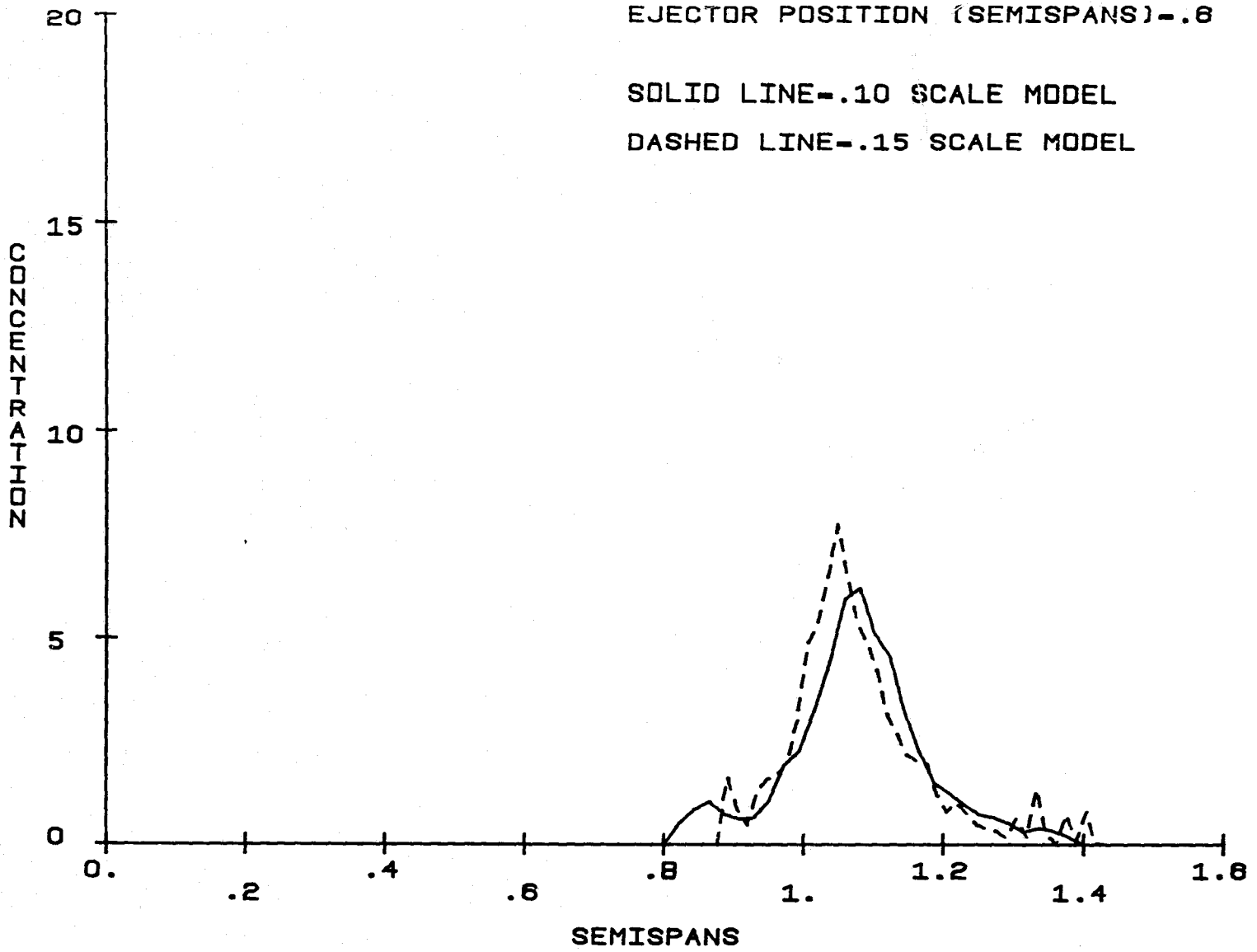
EJECTOR POSITION (SEMISPANS)=.8
SOLID LINE=.10 SCALE MODEL
DASHED LINE=.15 SCALE MODEL
CONCENTRATION
20
15
10
5
0
0.
.2
.4
.6
.8
1.
1.2
1.4
1.8
SEMISPANS

Figure 14(b).

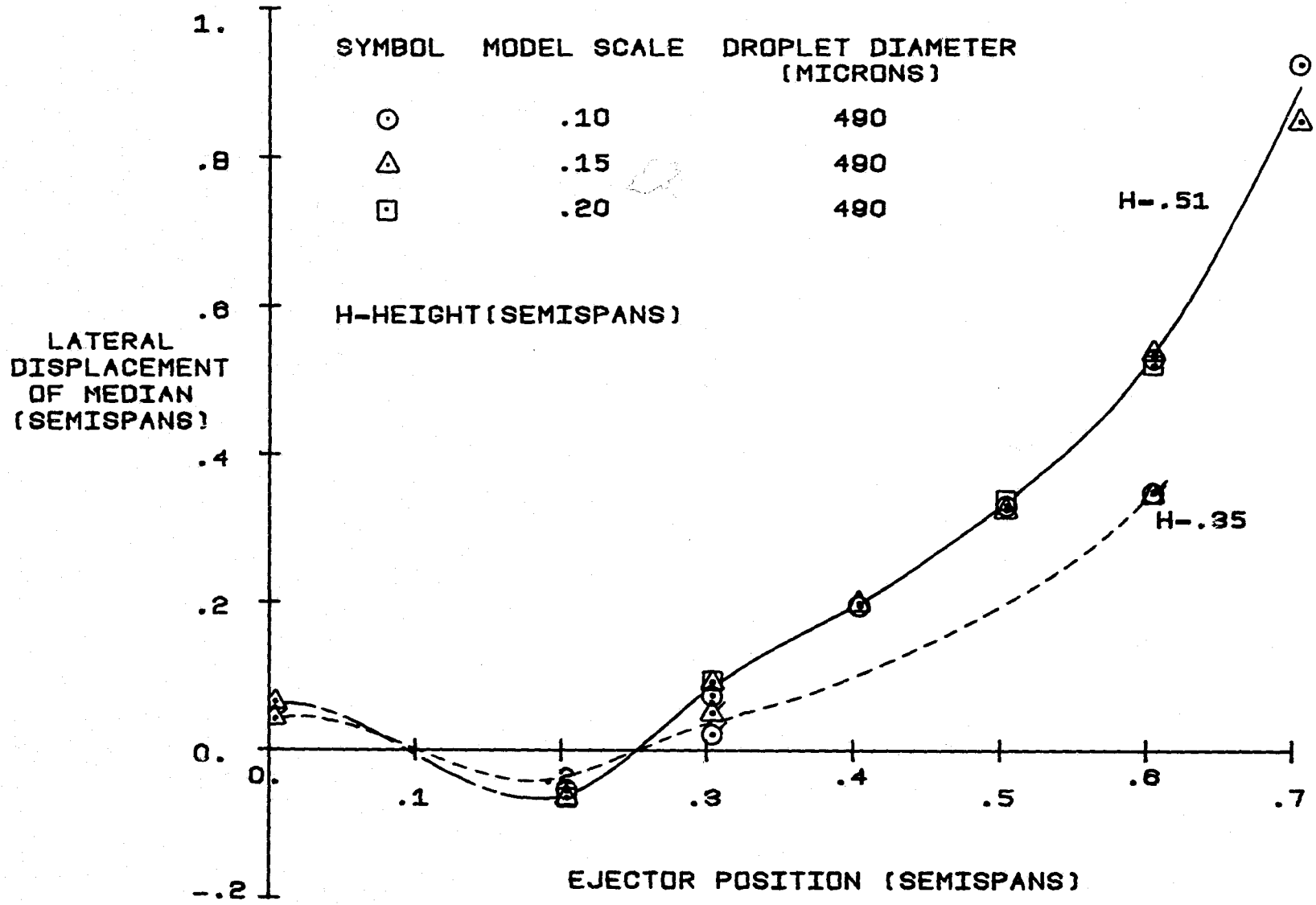

Figure 15. Lateral Displacement of the Deposition Median as a Function of the Ejector Position for Varying Model Heights. C_L = 0.61, Particle Size = 490 (Microns)

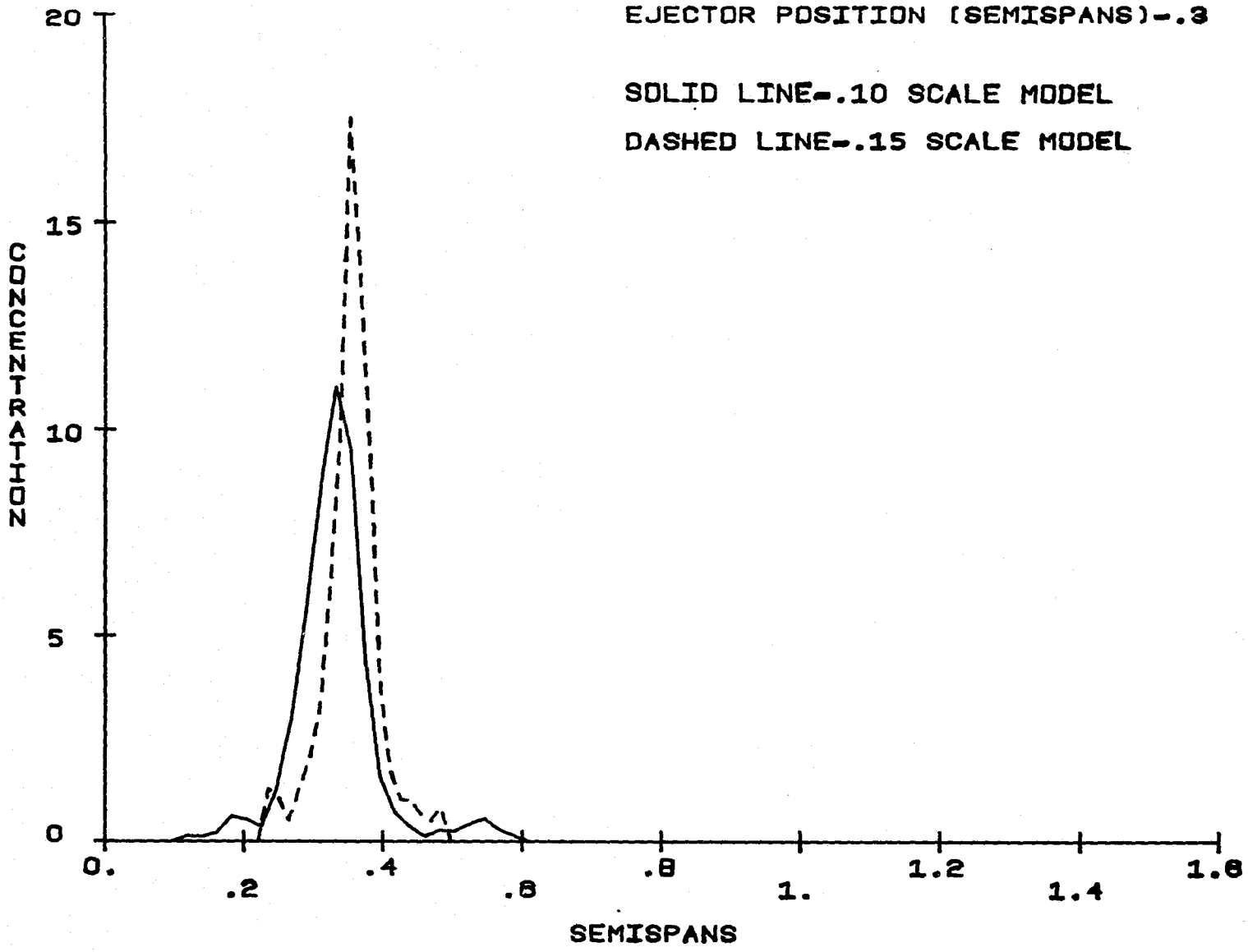

Figure 16(a). Deposition Patterns for the Scaling Law Validation Experiments with $\bar{H}$ = 0.35 (Semispans), C_L = 0.61, Particle Size = 490 (Microns)

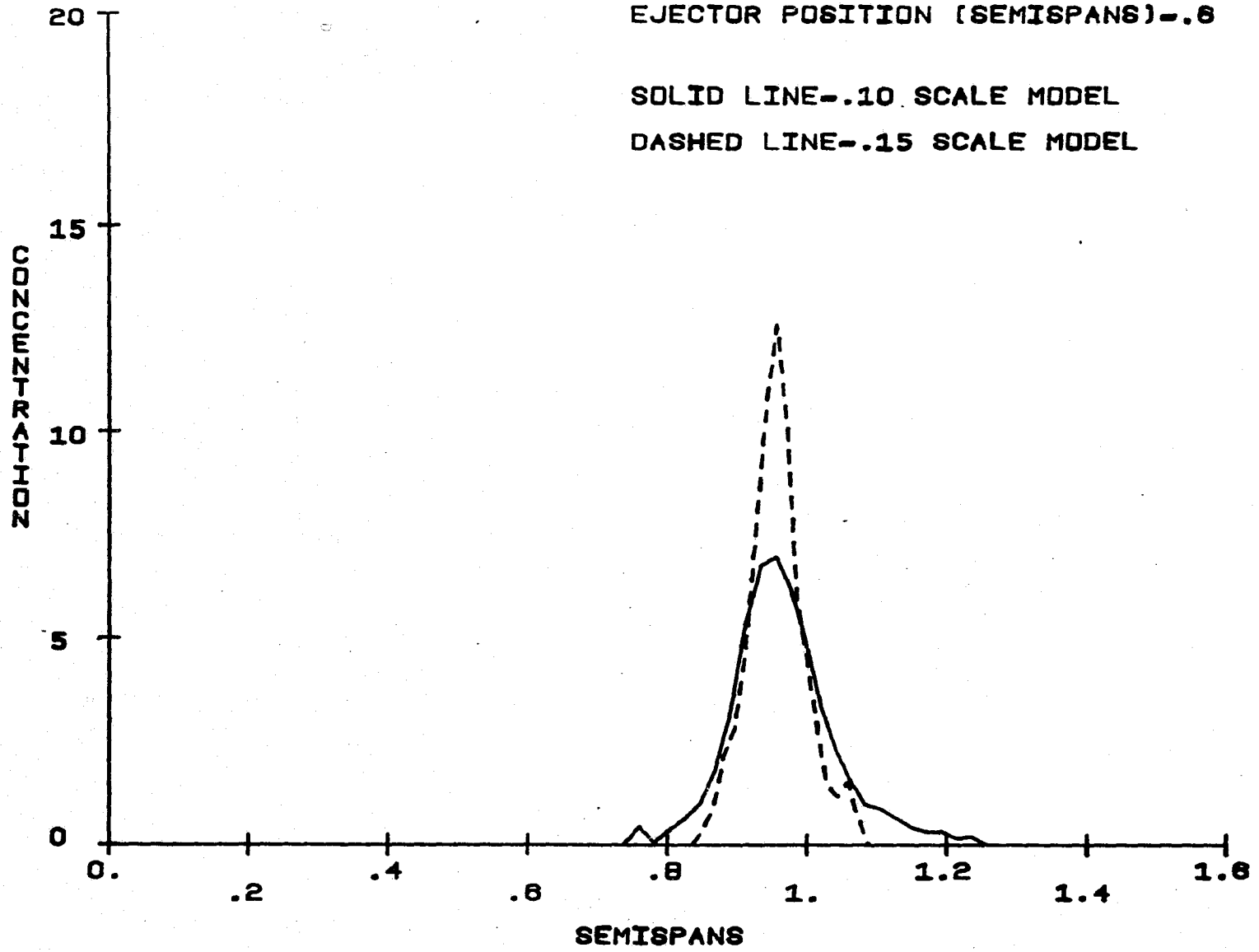
EJECTOR POSITION (SEMISPANS)=.6
SOLID LINE=.10 SCALE MODEL
DASHED LINE=.15 SCALE MODEL
CONCENTRATION
20
15
10
5
0
0.
.2
.4
.6
.8
1.
1.2
1.4
1.6
SEMISPANS

Figure 16(b).

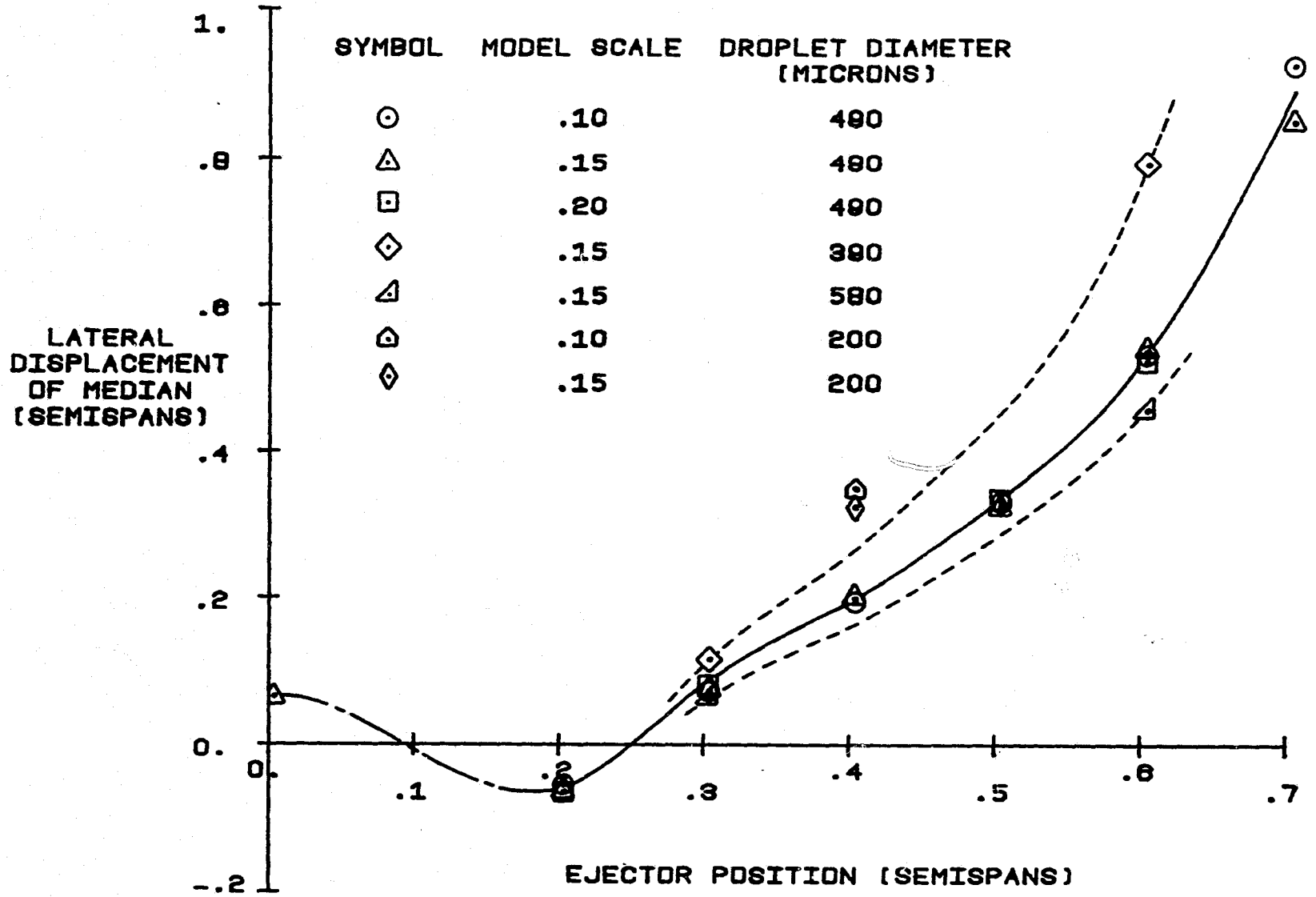

Figure 17. Lateral Displacement of the Deposition Median as a Function of the Ejector Position for Varying Particle Sizes. C_L = 0.61, H = 0.51 (Semispans); H = 0.35 (Semispans) for the Particle Size = 200 (Microns) Case

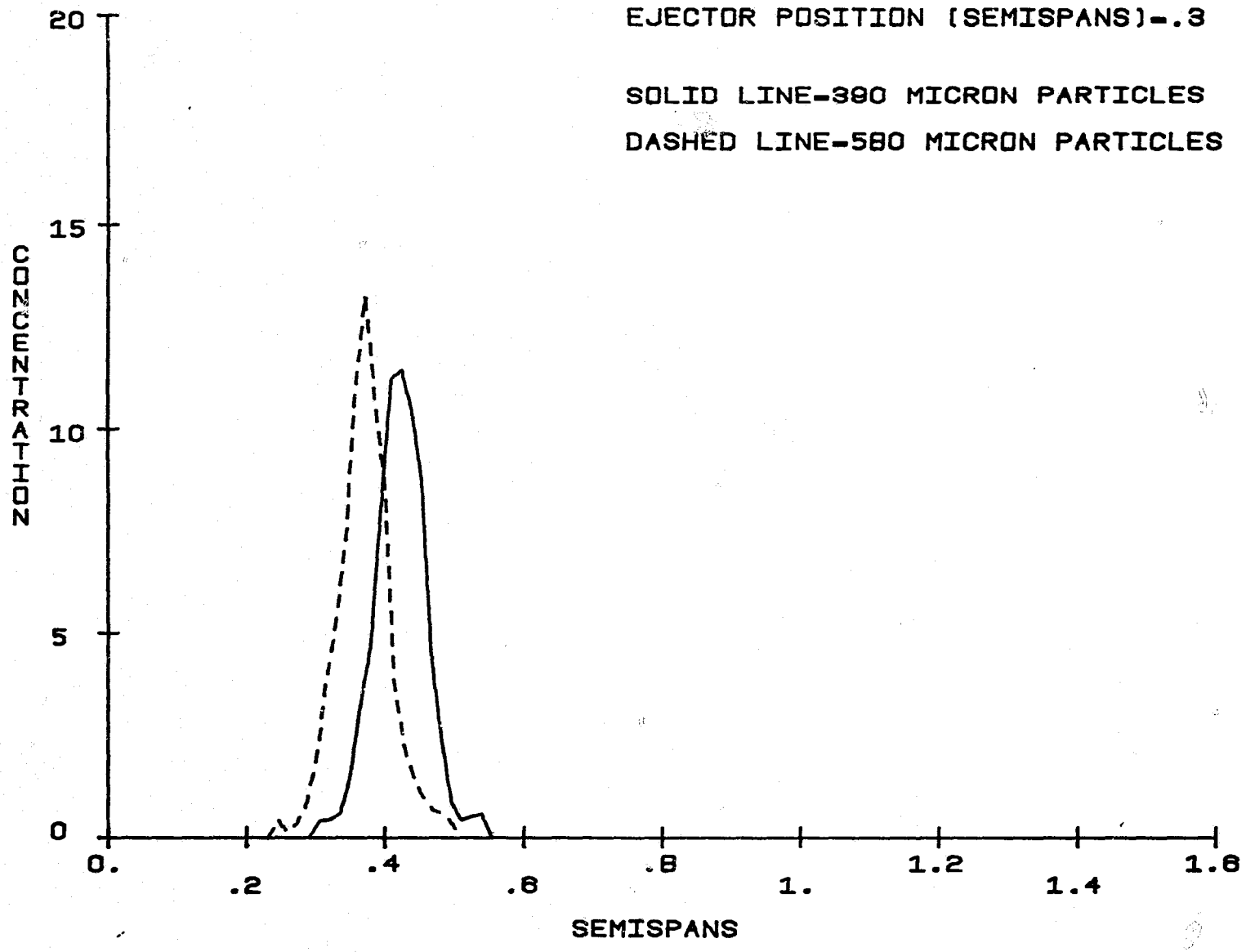

Figure 18(a). Deposition Patterns for the Scaling Law Validation Experiments with Varying Particle Sizes.
H = 0.51, C_L = 0.61

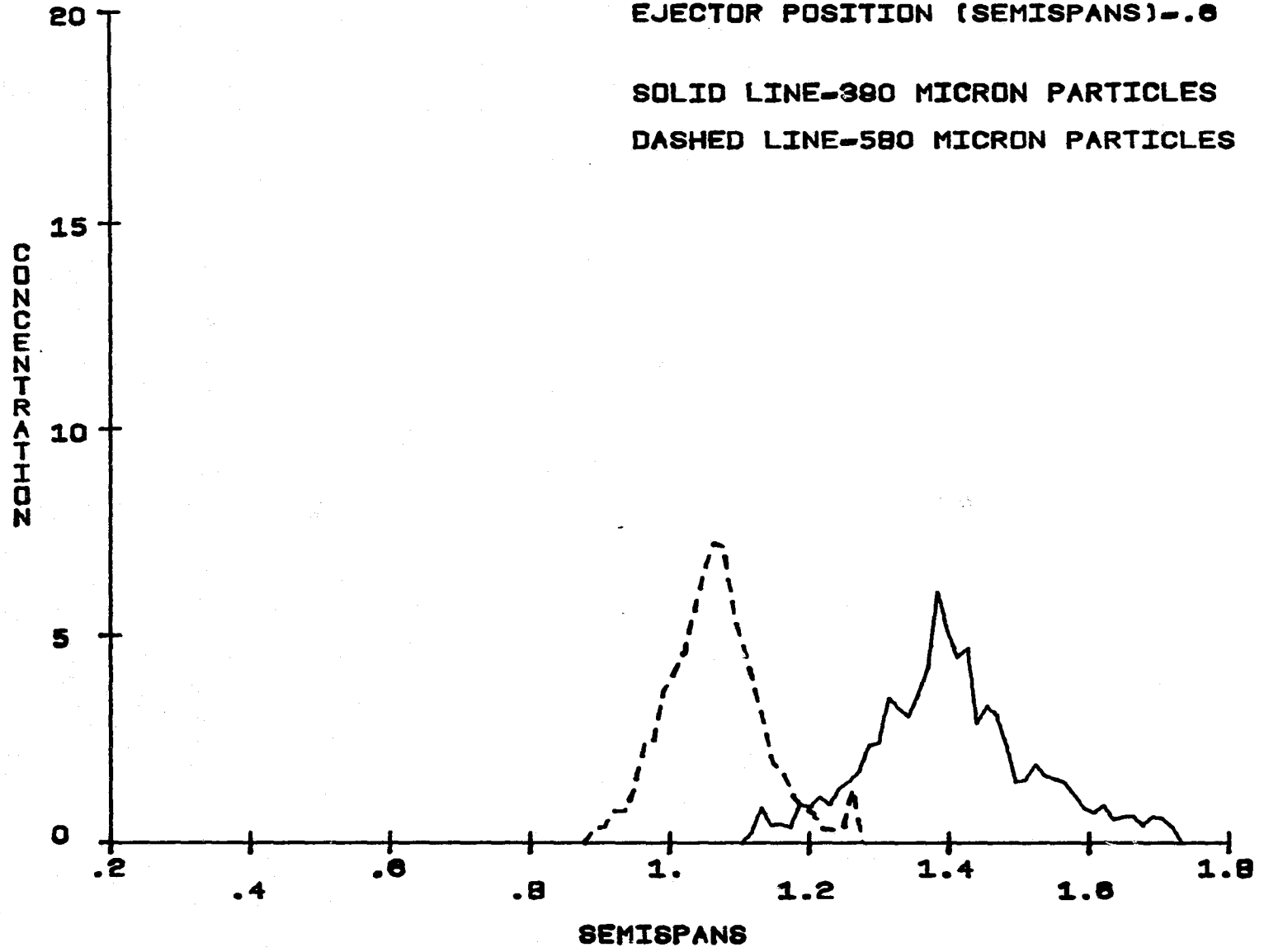
EJECTOR POSITION (SEMISPANS)=.6
SOLID LINE=380 MICRON PARTICLES
DASHED LINE=580 MICRON PARTICLES
CONCENTRATION
20
15
10
5
0
.2
.4
.6
.8
1.
1.2
1.4
1.6
1.8
SEMISPANS

Figure 18(b).

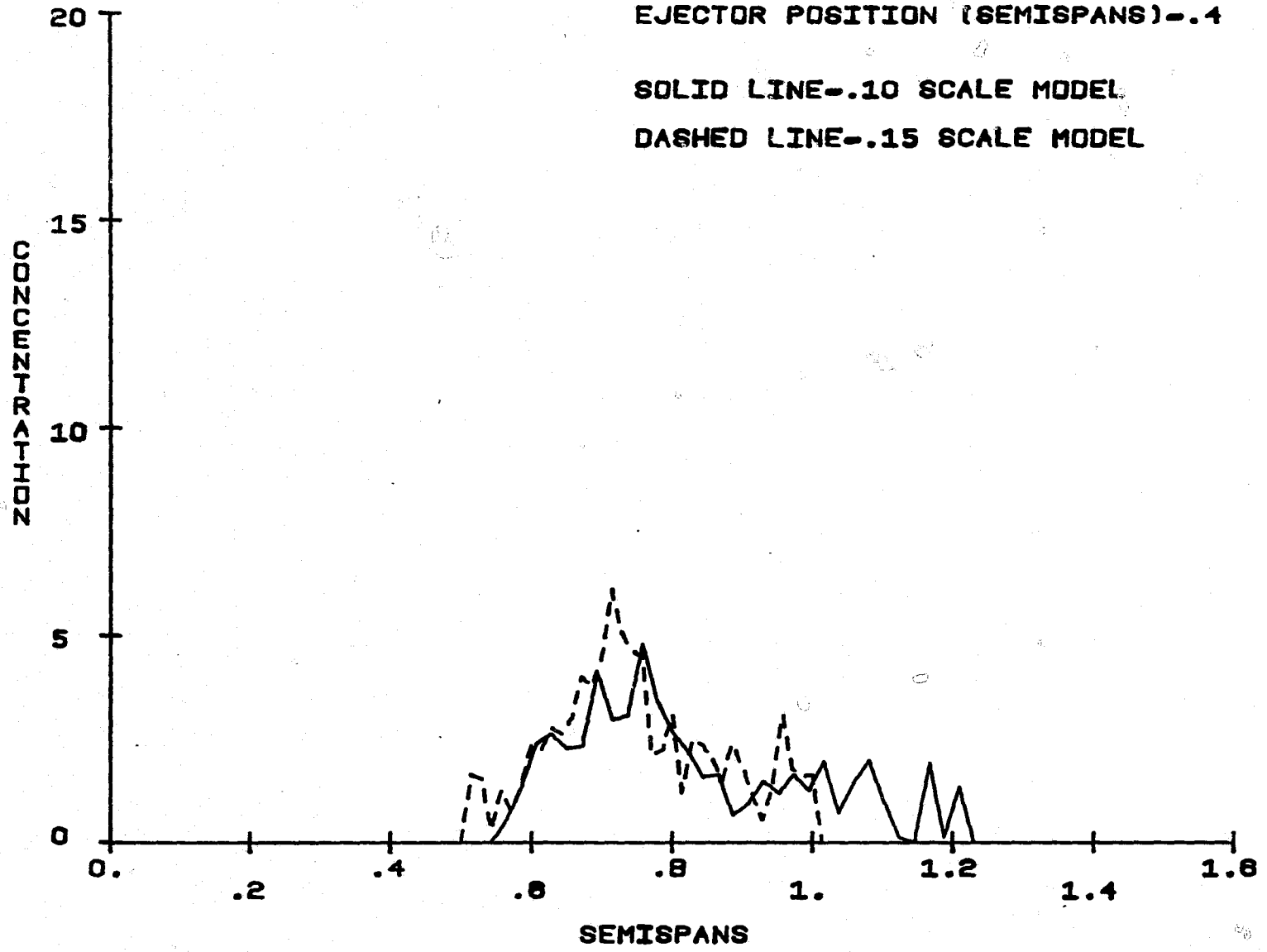

Figure 19. Deposition Patterns for the Scaling Law Validation Experiments with Particle Size = 200 (Microns), H = 0.35 (Semispans), C_L = 0.61

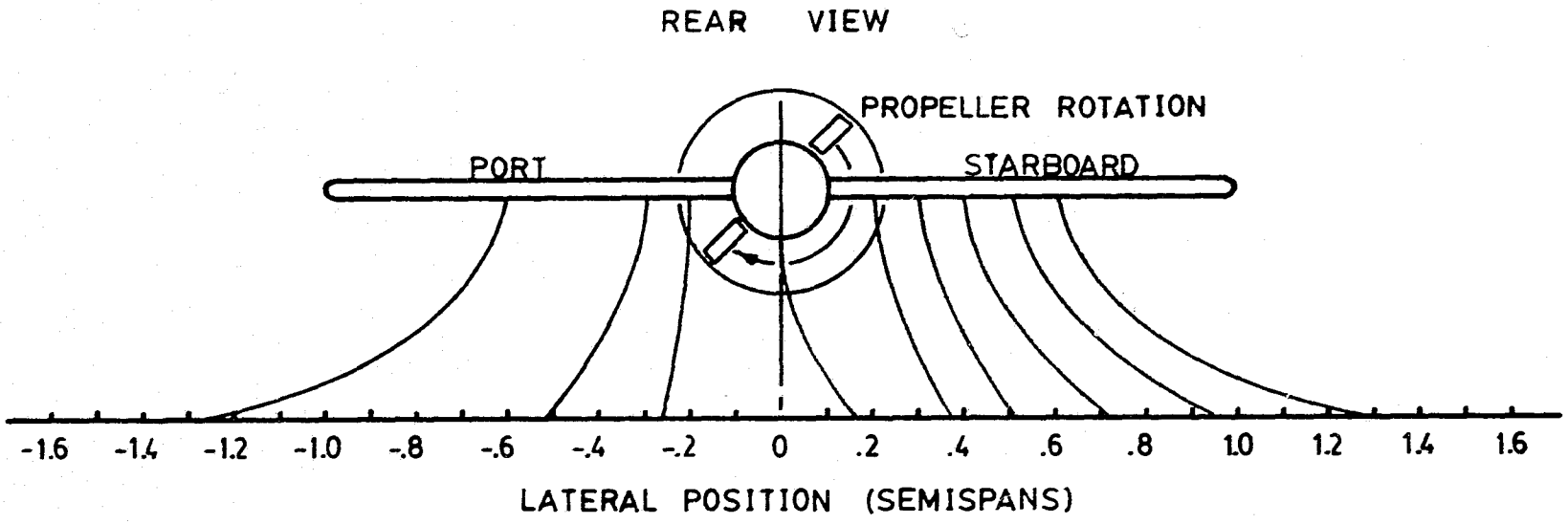

Figure 20. Median Deposition Trajectories for the Prop-on Baseline Scaling Law Validation Experiments. H = 0.51 (Semispans), C_L = 0.75, Particle Size = 490 (Microns)

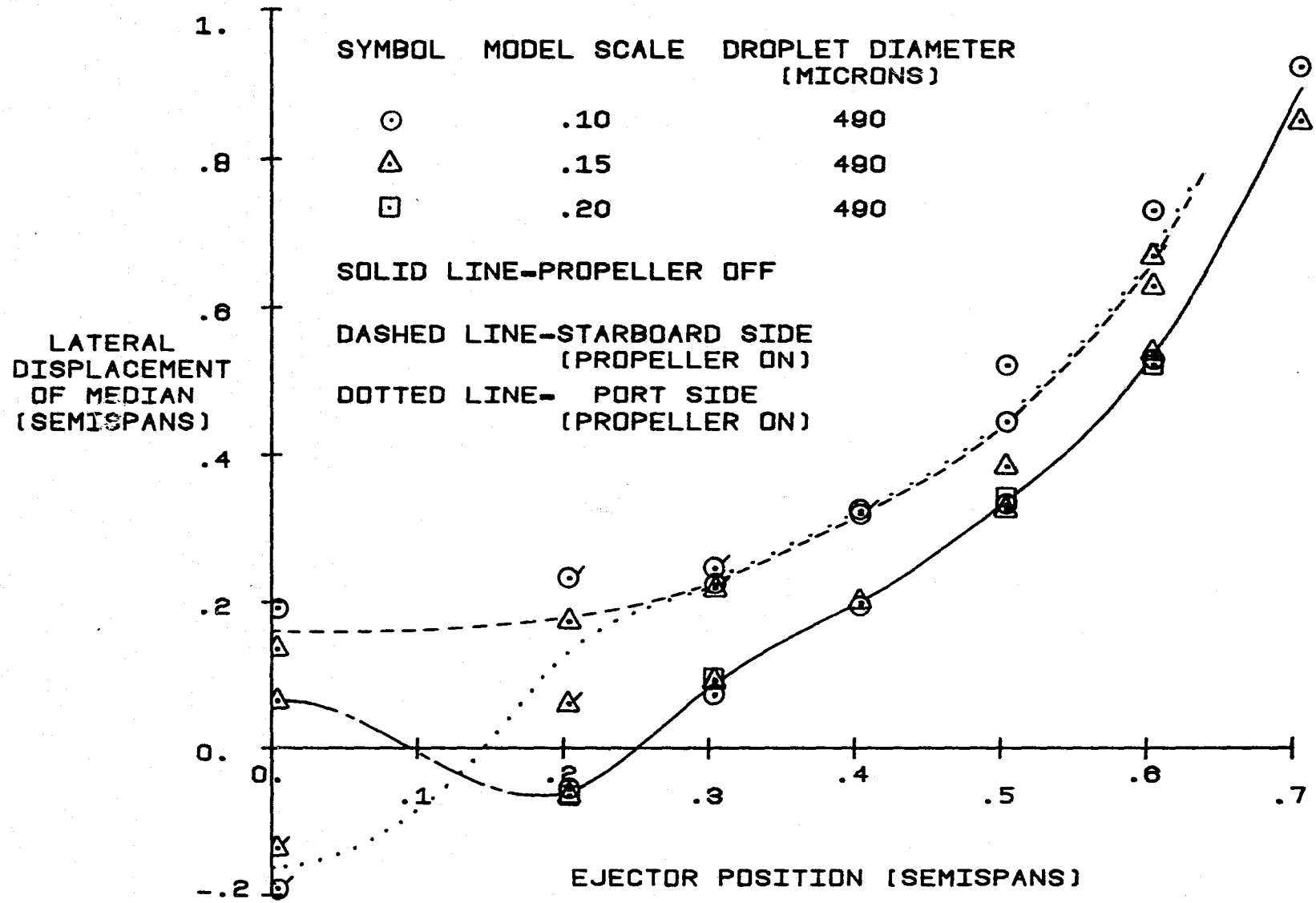

Figure 21. Lateral Displacement of the Deposition Median as a Function of the Ejector Position for the Baseline Scaling Law Validation Experiments. H = 0.51 (Semispans), $C_L \approx 0.75$ Prop-on Cases, Particle Size = 490 (Microns)

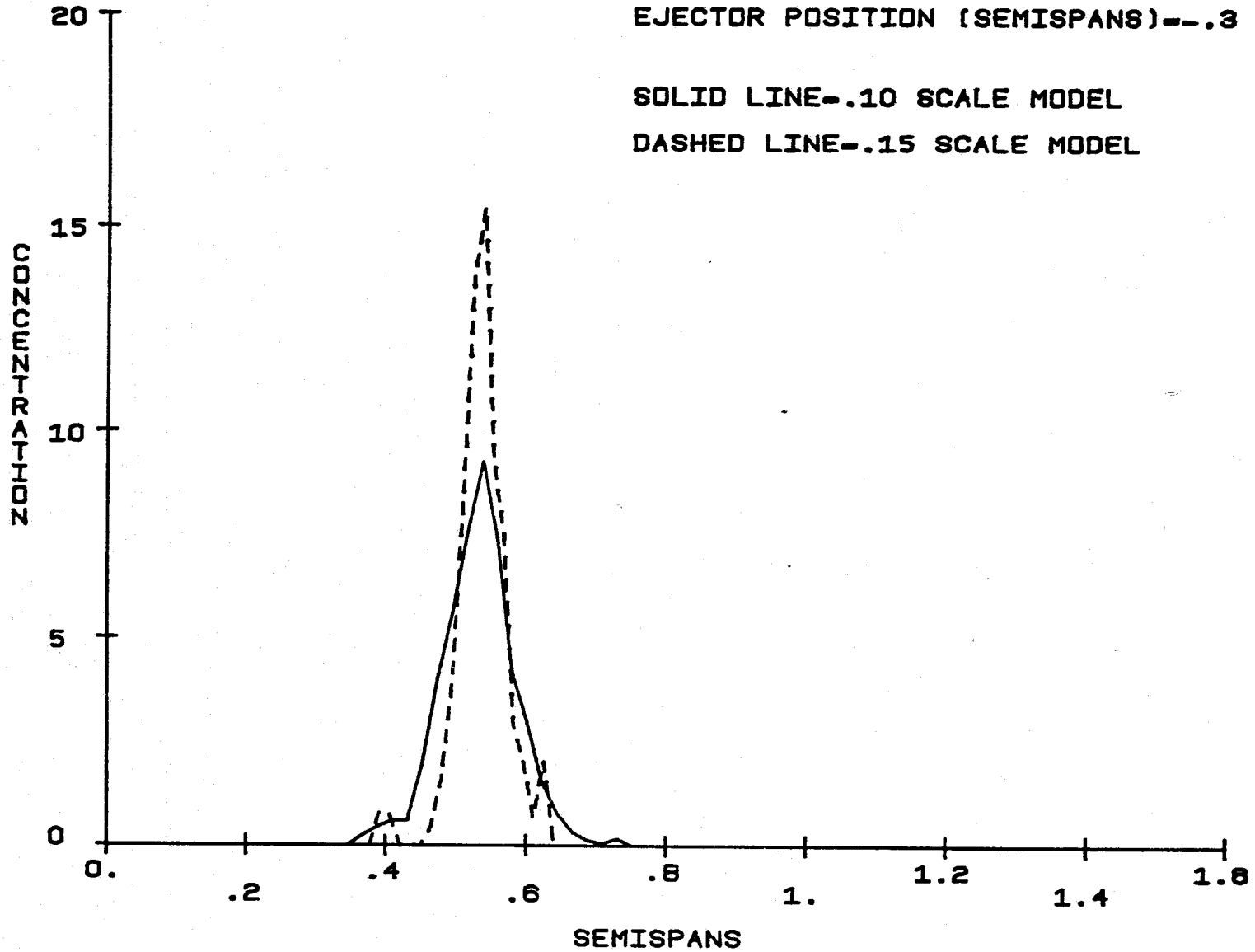

Figure 22(a). Deposition Patterns for the Baseline Prop-on Scaling Law Validation Experiments. H = 0.51 (Semispans), $C_L \approx 0.75$, Particle Size = 490 (Microns)

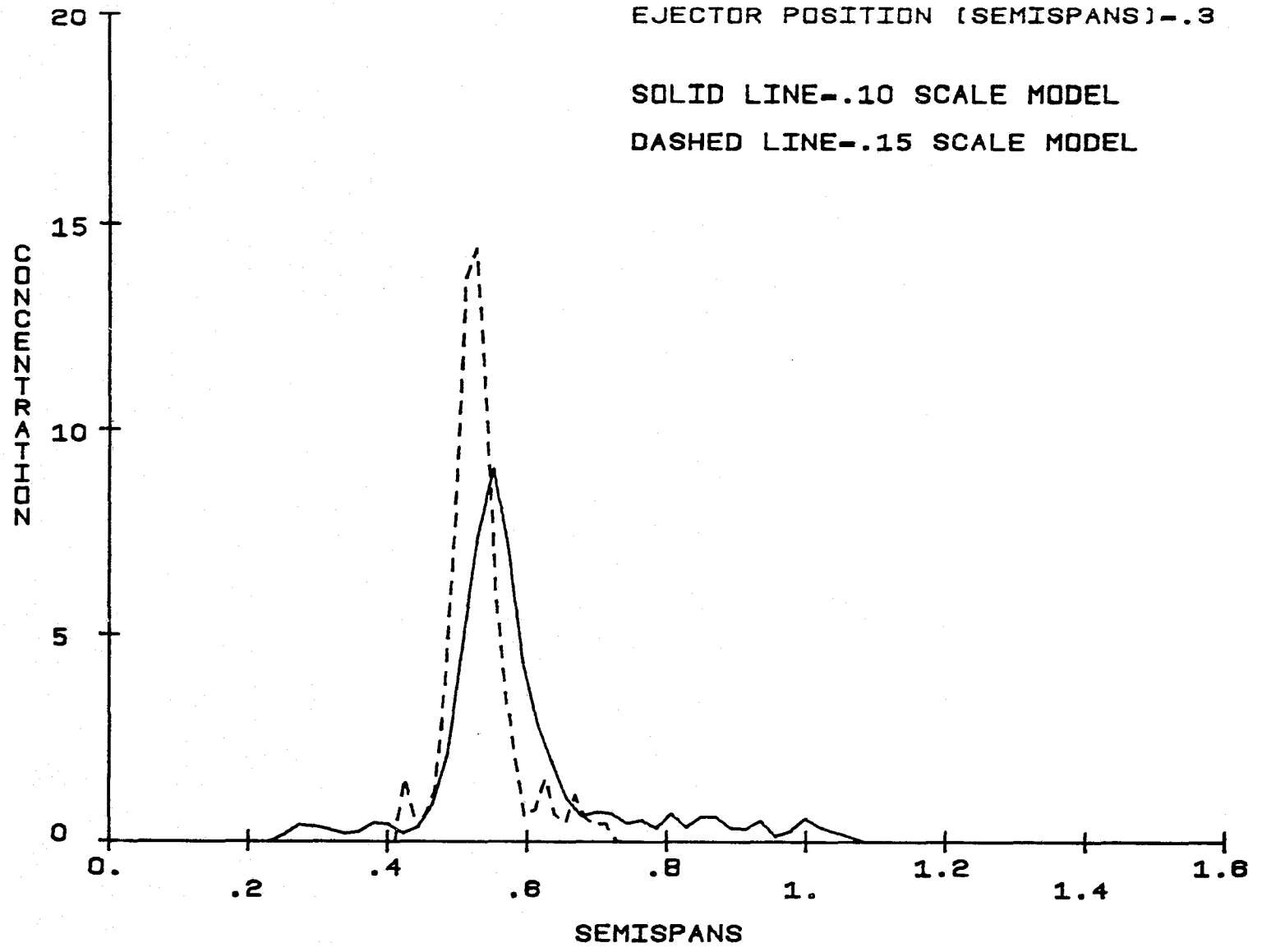
EJECTOR POSITION (SEMISPANS)=.3
SOLID LINE=.10 SCALE MODEL
DASHED LINE=.15 SCALE MODEL
CONCENTRATION
20
15
10
5
0
0.
.2
.4
.6
.8
1.
1.2
1.4
1.6
SEMISPANS

Figure 22(b).

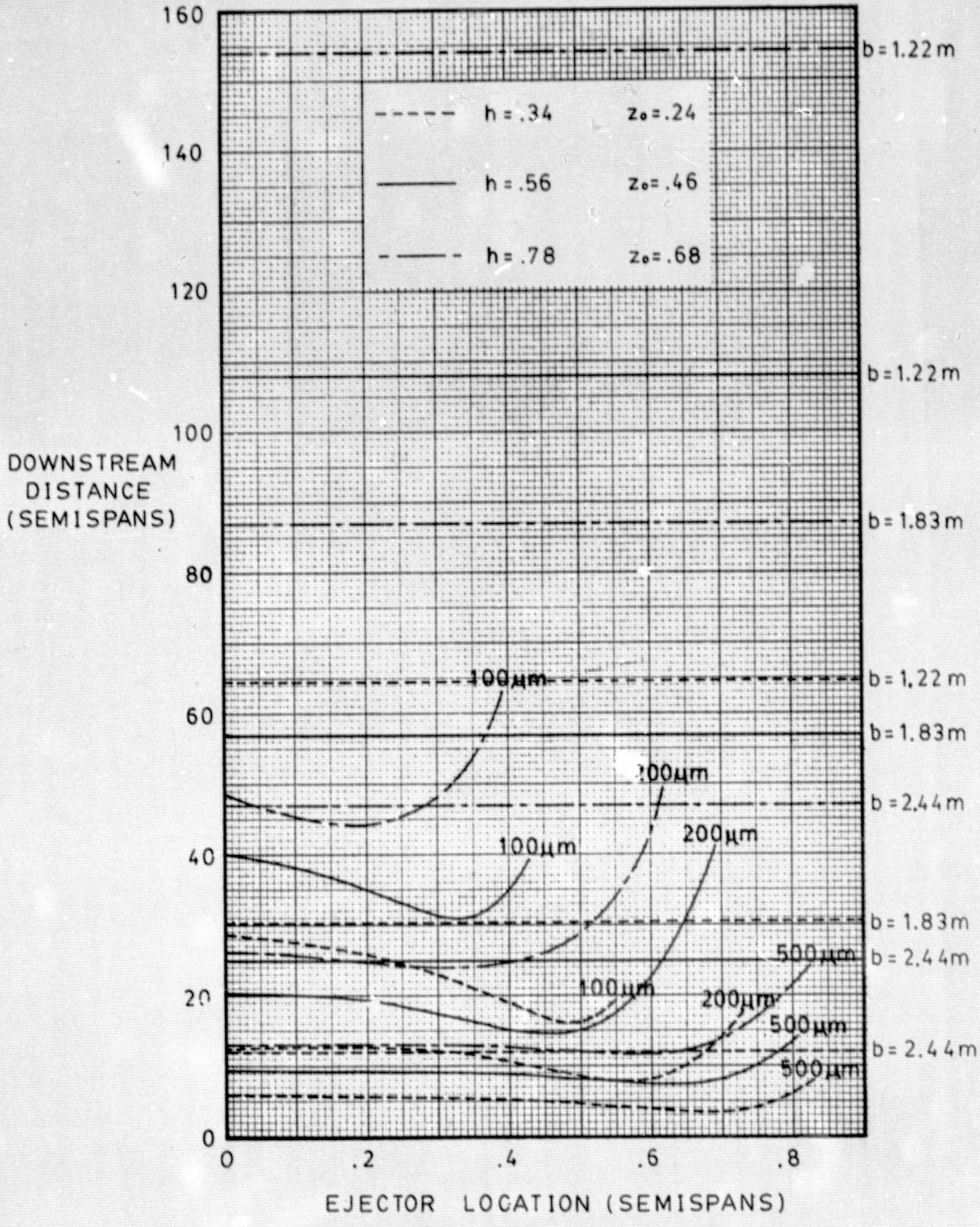

Figure 23. Facility Test Envelope for Varying Model Heights.
AR = 6.0, U_∞(full-scale) = 47.2 m/sec, C_L = 0.54

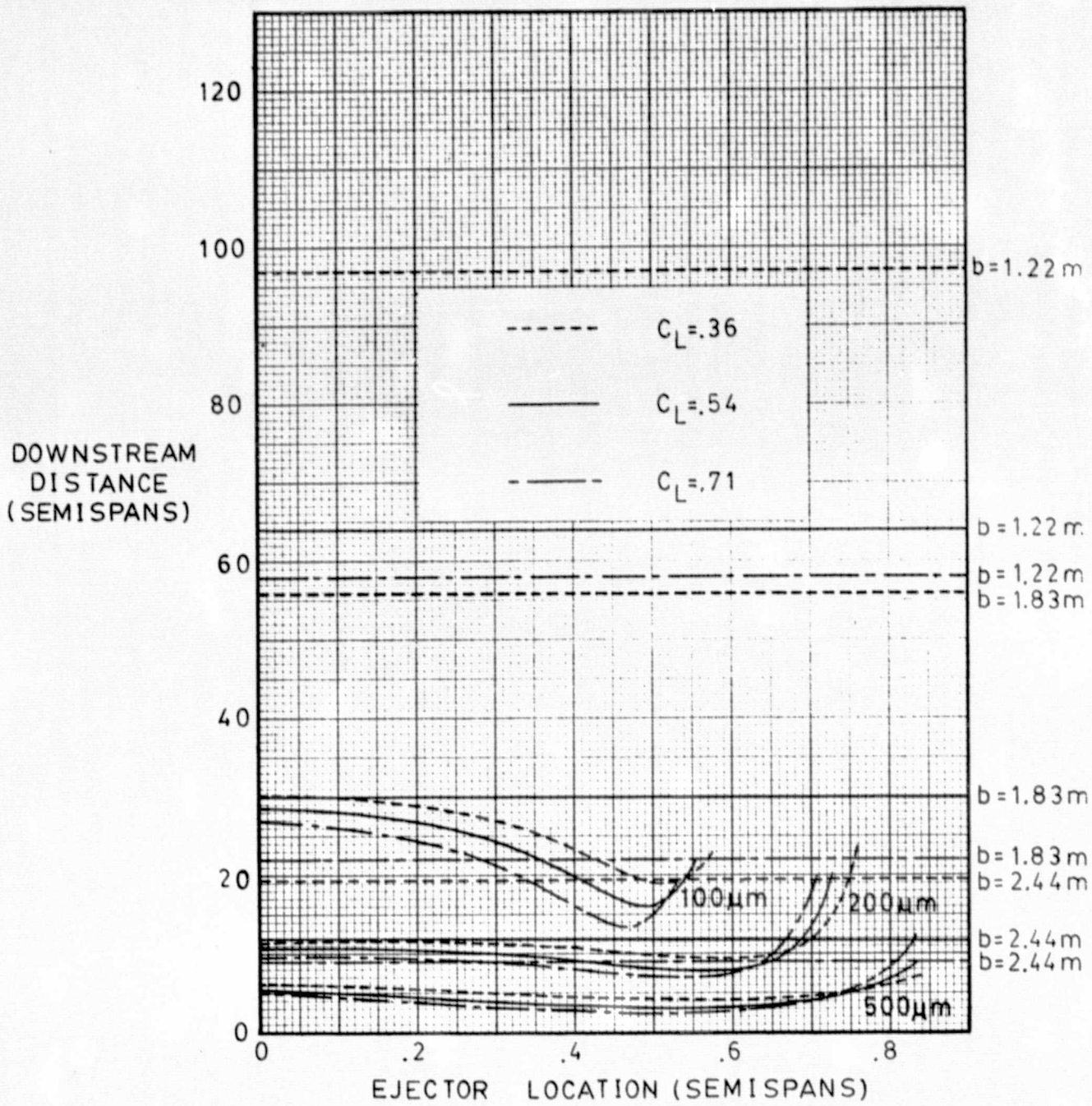

Figure 24. Facility Test Envelope for Varying Lift Coefficients. AR = 6.0, U_∞ (full-scale) = 47.2 m/sec, H = 0.34, z_o = 0.24

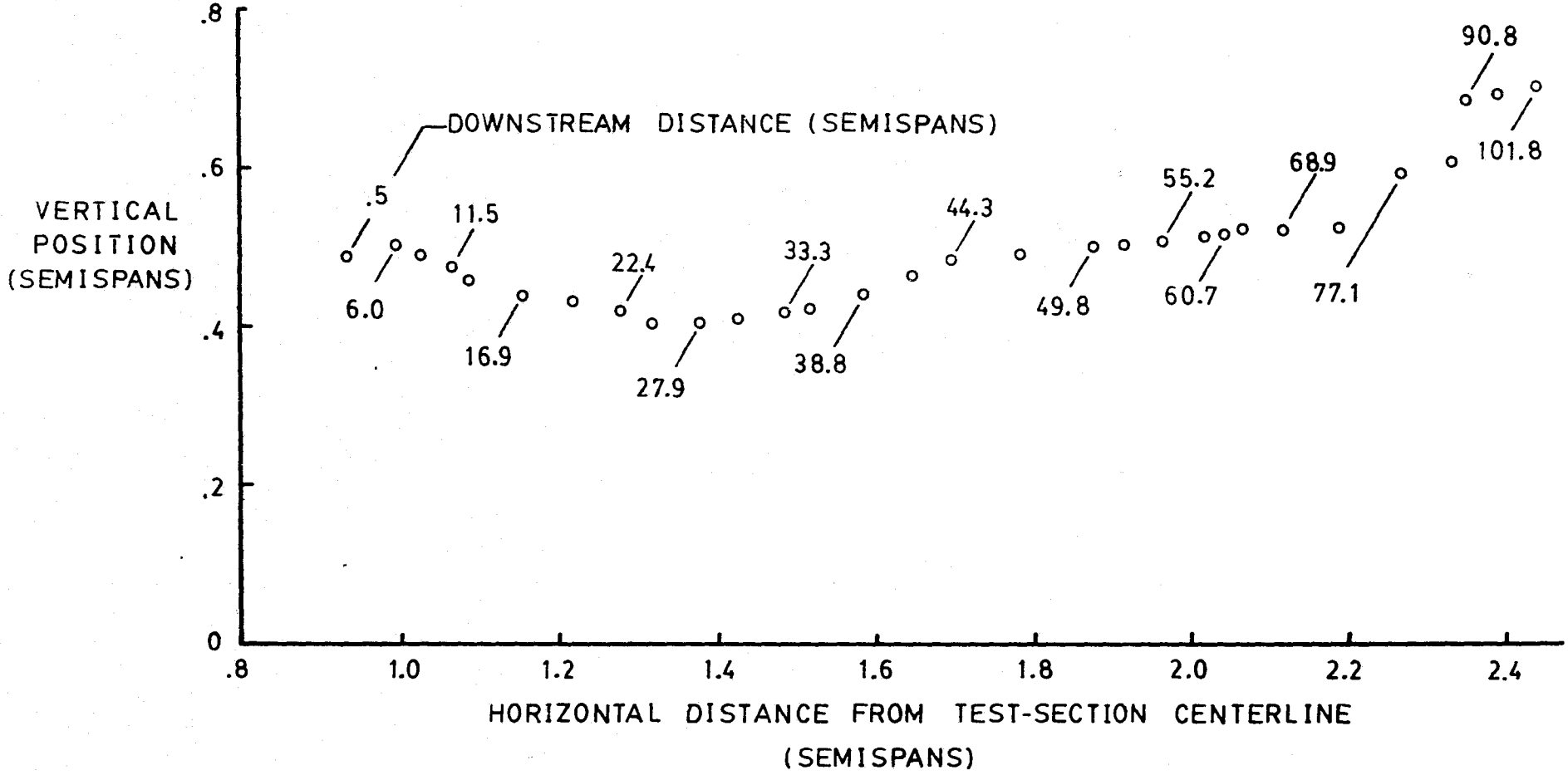

Figure 25. Typical Vortex Trajectory for the 1.22 Meter Span Model. Test Section Wall at 4.51 Semispans, C_L = 0.6, Model Velocity = 16.8 m/sec

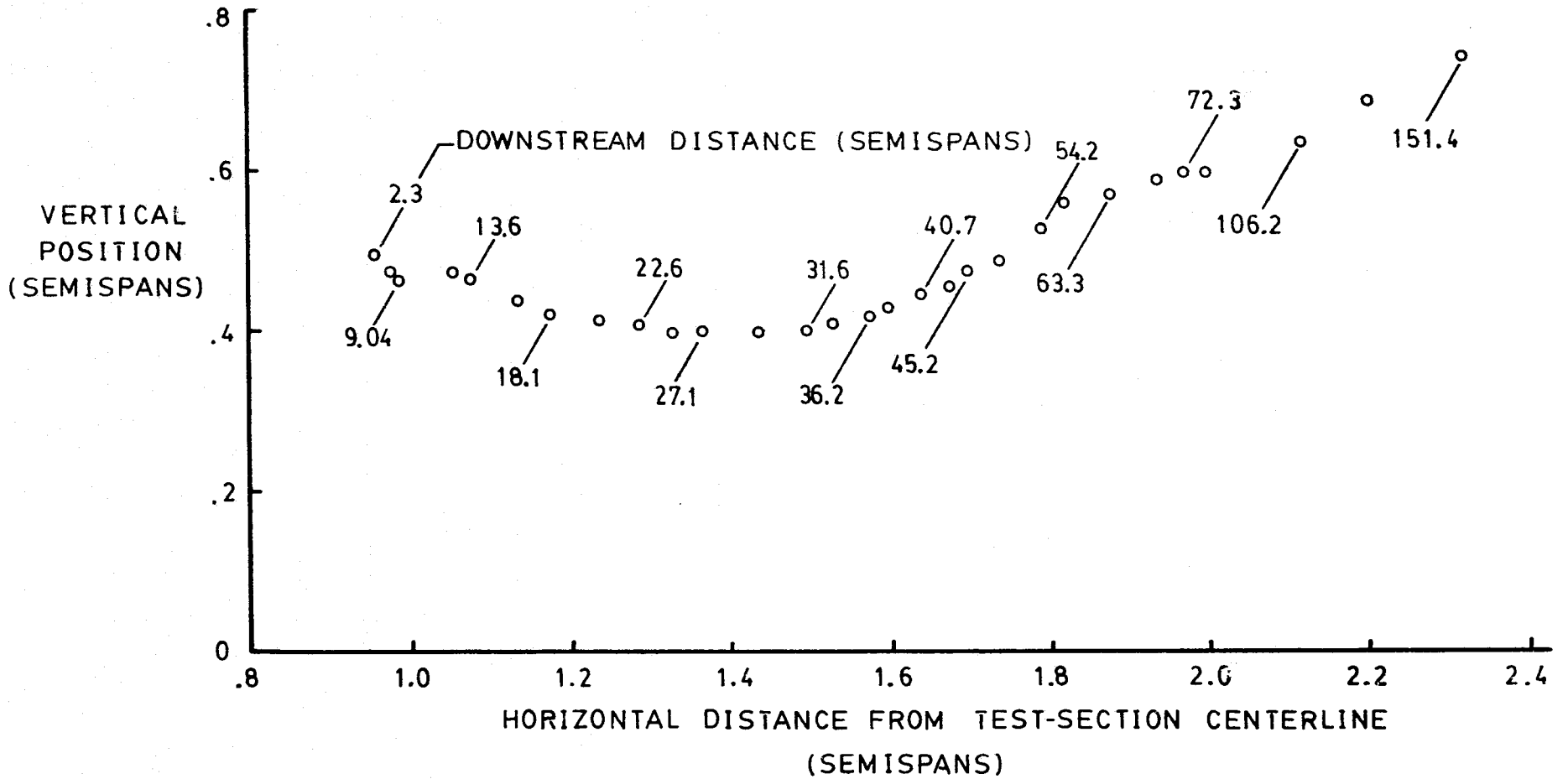

Figure 26. Typical Vortex Trajectory for the 1.83 Meter Span Model. Test Section Wall at 3.01 Semispans, C_L = 0.6, Model Velocity = 20.9 m/sec

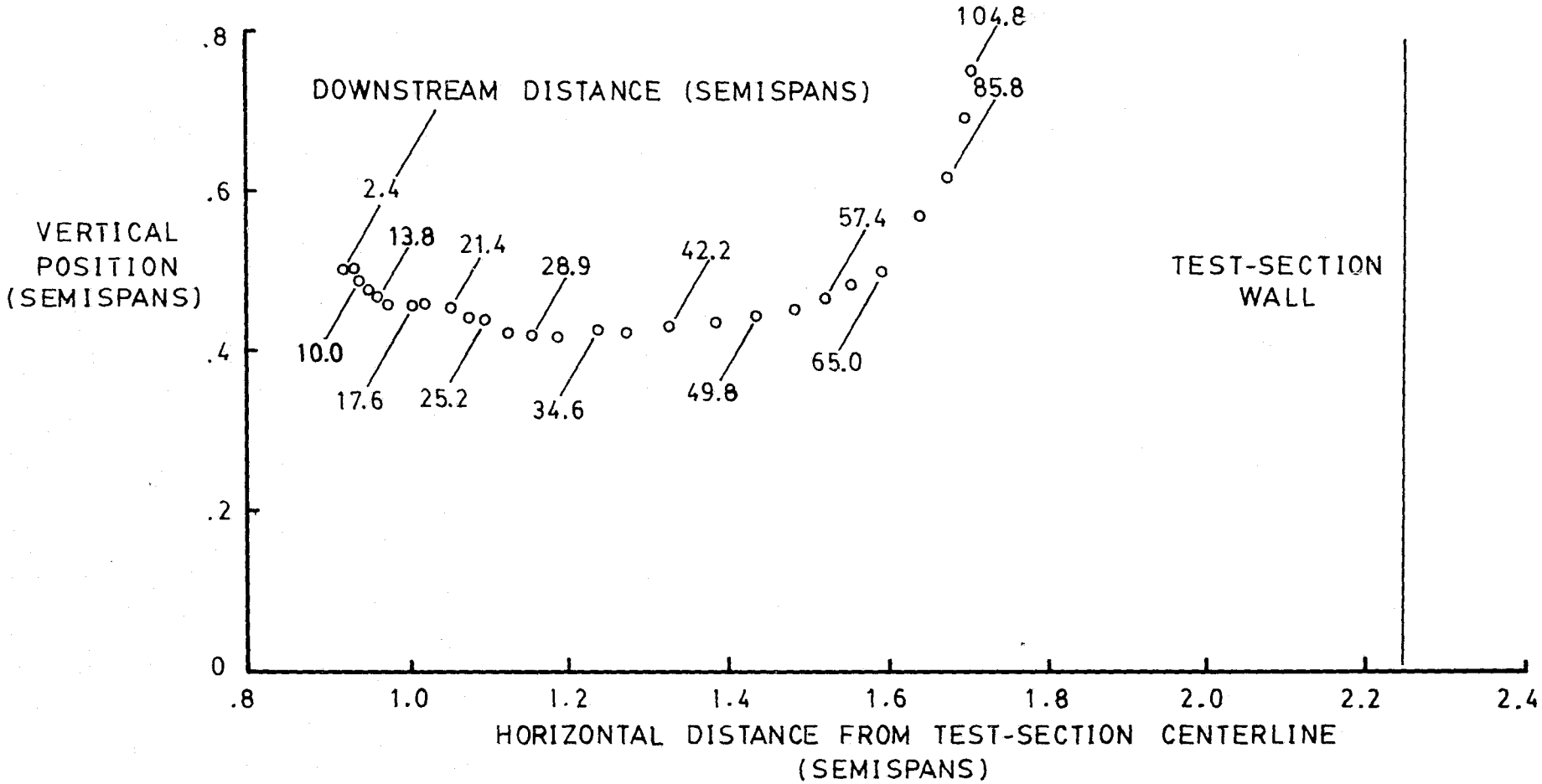

Figure 27. Typical Vortex Trajectory for the 2.44 Meter Span Model. Test Section Wall at 2.25 Semispans, C_L = 0.6, Model Velocity = 23.6 m/sec